Mineralium Deposita (1998) 33: 437–460

ARTICLE

P. Buchholz · P. Herzig · G. Friedrich · R. Frei

Granite-hosted gold mineralization in the Midlands greenstone belt: a new type of low-grade gold deposit in Zimbabwe

Received: 29 January 1997 / Accepted: 22 September 1997

Abstract In 1992, the Ford gold deposit was rediscovered during field work in the Kwekwe district near the Indarama mine, approximately 200 km southwest of Harare, Zimbabwe. Based on diamond drilling and open pit operations, estimated ore reserves are at least 3 Mt with an average gold content of 2.5 g/t. The gold deposit is located within a porphyritic granite dike with a thickness of 20–50 m, striking 800 m NNW-SSE. It dips 60–70° to the NE and intrudes a volcano-sedimentary sequence of tholeiitic basalts, acid volcanics, and banded iron formations of the Bulawayan Group (2900–2700 Ma). The intrusion of the dike occurred at 2541 ± 17 Ma (Pb/Pb step leaching technique) within a second order structure and is related to displacement along transcrustal deformation zones such as the Sherwood- and Taba-Mali deformation zones. Gold mineralization is confined to the s-shaped part of the dike intrusion. At the present stage of mining, the deposit is characterized by the absence of major veins, the occurrence of disseminated pyrite throughout the orebody, and a distinct alteration pattern comparable to that of porphyry copper deposits. The central zone of the dike shows a typical K-feldspar-albite-sericite-pyrite (± biotite?) alteration, followed by a narrow external propylitic zone. Native gold with an average Ag content of 5 wt.% and a grain size of 5–100 μm is rare and occurs within pyrite and secondary K-feldspar. Sulphide mineral separates of pyrite and minor arsenopyrite probably contain invisible gold (up to 120 ppm) amenable to cyanidation. Anomalously high gold values of ~7 ppm have been found in the transition between the K-feldspar-albite-sericite-pyrite alteration and the propylitic zone, indicating that the mineralizing fluids have experienced major physico-chemical changes in the transition zone. The regional tectonic position of the orebody suggests that the emplacement of the granite and the gold mineralization are structurally controlled. The Pb isotope composition of several leachates of pyrite indicate isotope disequilibrium with magmatic minerals and point to a contamination of the mineralizing fluid by Pb from older (sedimentary?) sources. Stable isotope geochemistry of sulphides and carbonates as well as the metallogeny of the deposit compare to shear-zone hosted gold mineralization in the Kwekwe district, for which a deep crustal origin has been discussed. Although this study documents contrasting evidence for a porphyry-gold versus a shear-zone type of mineralization, it is suggested that gold-bearing fluids were syntectonically introduced into a ductile shear zone within the granite dike either during cooling of the intrusion or later in Archaean or early Proterozoic times.

Editorial handling: A.C. Brown

P. Buchholz (✉) · P. Herzig
Lehrstuhl für Lagerstättenlehre, Institut für Mineralogie,
Technische Universität Bergakademie Freiberg,
Brennhausgasse 14, D-09596 Freiberg, Germany

G. Friedrich
Institut für Mineralogie und Lagerstättenlehre,
Rheinisch-Westfälische Technische Hochschule Aachen,
Wüllnerstr. 2, D-52056 Aachen, Germany

R. Frei
Mineralogisch-Petrographisches Institut,
Gruppe Isotopengeologie, Universität Bern, Erlachstrasse 9A,
CH-3012 Bern, Switzerland

Introduction

The central part of the Midlands greenstone belt is one of the largest gold districts in Zimbabwe and, on a world scale, represents a major province of vein and shear-zone hosted gold- and gold-antimony deposits. During the past ten years, the Midlands greenstone belt has been the subject of several exploration and research programs because of its high potential for gold resources (Foster et al. 1986; Foster et al. 1991; Arita and Sato 1987; Nutt et al. 1988a,b; Pitfield and Campbell 1990, 1993; Pitfield et al. 1991; Carter 1990; Porter and Foster 1991; Buchholz et al. 1994; Buchholz 1995; Campbell

and Pitfield 1994). In April 1992, the Ford deposit was rediscovered and re-examined after more than 60 years of abandonment during a research program on gold mineralization in the Kwekwe district, commissioned and funded by the German Federal Institute for Geosciences and Natural Resources (Buchholz et al. 1993; Friedrich et al. 1996). Mining operations were started by Boulder Mining Company (PVT) Ltd in 1993. Mining activities in the old "Ford Section" of the Taba Mali Group of mines date back to the 1930s, but major gold production has not been recorded. The Ford mine is located about 10 km north of the town of Kwekwe, about 200 km southwest of Harare (18°50′S, 29°46′E) (Fig. 1). At the current stage of exploration and mining, estimated resources are at least 6 Mt of ore with an average grade of 2.5 g/t Au. The ore is mined in an open pit operation (~600 t/day) (Fig. 4) and processed at the nearby Indarama/Broomstock mine site. Gold is extracted by carbon-in-pulp cyanide leaching, with a recovery of ~90%.

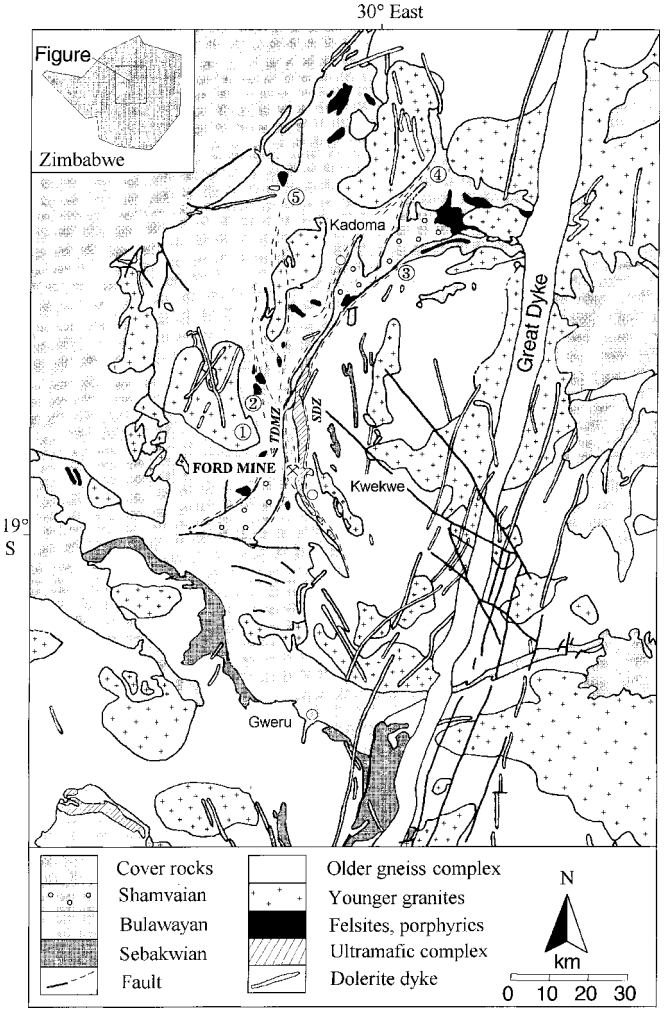

Fig. 1 Simplified geological map of the Midlands greenstone belt with location of the granite-hosted gold mineralization at the Ford mine near Kwekwe (*1*, Sesombi tonalite; *2*, Hatchland porphyritic intrusion; *3*, Munyati Deformation Zone; *4*, Kadoma Deformation Zone; *5*, Lily Deformation Zone; *SDZ*, Sherwood Deformation Zone; *TMDZ*, Taba Mali Deformation Zone)

Mineralization at the Ford mine is not spatially related to major veins as are many other gold deposits in the Kwekwe district. Instead, gold and sulphides are disseminated throughout the orebody within an s-shaped granite dike. Because of this, the spatial relationship to a porphyritic intrusion, and the uncommon alteration pattern, a possible genetic relationship to porphyry type deposits is discussed. Similar dikes are common in the area and some of them carry gold as well.

The majority of porphyry copper-gold and copper-deficient porphyry gold deposits was generated at Phanerozoic convergent plate margins (Sillitoe 1991; Vila et al. 1991). The existence of Archaean gold-bearing porphyry deposits has been discussed for the Norseman-Wiluna greenstone belt in Western Australia (Perring et al. 1991; Perring and McNaughton 1992) and the Abitibi belt in Canada (Sinclair 1980; Issigonis 1980; Cameron and Hattori 1987; Hattori 1987; Burrows and Spooner 1989; Spooner 1991; Fraser 1993 and therein). The Ford mine in the Midlands greenstone belt, Zimbabwe, shows features typical of both porphyry and shear-zone related gold deposits, and leads to a new discussion of these two types of mineralization.

In this study, we report on the geologic setting and the geochemical features of mineralization and alteration at the Ford deposit. The results point to new exploration targets in the area and are possibly relevant to the search for granite-hosted gold mineralization in other Zimbabwean greenstone belts.

Regional geological setting

The Midlands and associated greenstone belts in Zimbabwe are terminated to the NE, E, and S by the early Archaean Rhodesdale granitoid-gneiss complex (older gneiss complex) and to the NW and W by later cover rocks of Proterozoic to Phanerozoic age (Fig. 1). The greenstone belt sequence comprises metavolcanic rocks of the Sebakwian Group (3500 Ma), tholeiitic metabasalt, calc-alkaline and bimodal volcanic rocks, as well as metasedimentary rocks of the Bulawayan Group (2900–2700 Ma), and metasedimentary rocks of the Shamvaian Group (2700 Ma). Rocks of the Shamvaian Group are discordant to the folded series of the Bulawayan Group and consist of a clastic succession of jaspilite breccias, conglomerates, banded iron formations (BIFs), and sandstones (Harrison 1970). Tonalites of the Sesombi suite intruded the greenstone belt in the late Archaean (younger granites, Fig. 1), e.g. the Sesombi tonalite ~30 km northwest of Kwekwe at 2570 ± 42 Ma (Rb/Sr; Darbyshire in Pitfield and Campbell 1993; 2690 ± 140, Hawkesworth et al. 1975). A few porphyritic intrusions occur within the greenstone sequence, but only one has been dated as yet (Hatchland intrusion, 2457 ± 65 Ma, Rb/Sr; Darbyshire in Pitfield and Campbell 1993).

Lithospheric shortening led to crustal thickening and the development of transcrustal strike slip and reverse shear zones in late Archaean/early Proterozioc times (Campbell and Pitfield 1994). Small gneiss bodies such as the Sebakwe gneiss at the Sebakwe river, south of the Ford mine, are evident for major reverse or thrust shearing and tectonic imbrication within the greenstone belt (Fig. 2). Second order dextral reverse and thrust shears have been

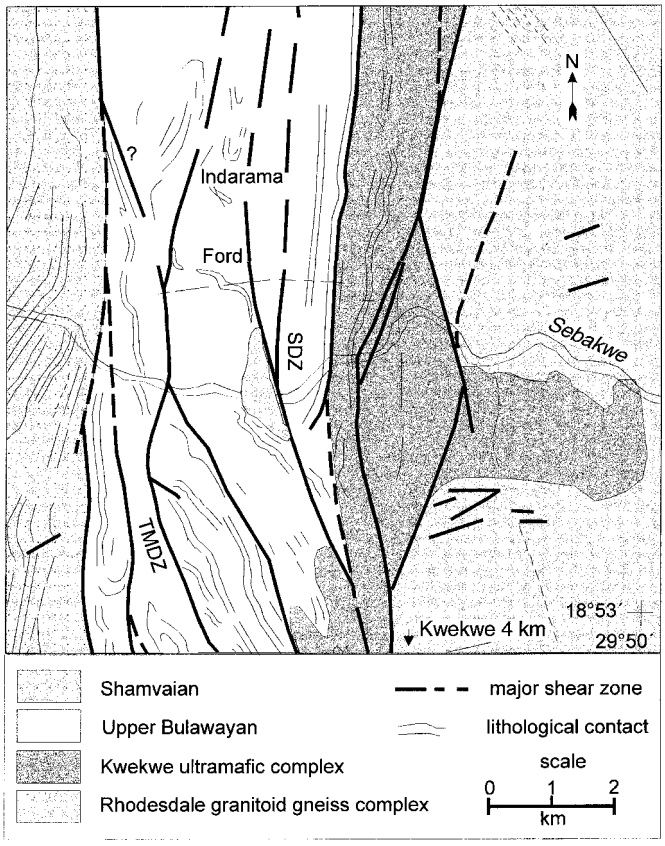

Fig. 2 Structural geological map of the Ford mine area, Kwekwe district (modified after Harrison 1970; Nutt et al. 1988a; Landsat Thematic Mapper image-supported structural geologic map of the Midlands greenstone belt by Campbell and Pitfield 1994)

observed in several mine locations, which indicate a regional change from a NW to W and SW orientated compressional tectonic regime (Campbell and Pitfield 1994). Interpretations of satellite images and air photographs indicate that the regional structure is dominated by N-S-trending transcrustal master shears in the Kwekwe district identified as the Sherwood (SDZ) and Taba Mali deformation zones (TMDZ, Figs. 1 and 2) (Campbell and Pitfield 1994). North of Kwekwe, the SDZ splits into three major splays, which run subparallel to the contact zone between the Rhodesdale granitoid-gneiss and the Kwekwe ultramafic complexes as well as within Upper Bulawayan volcano-sedimentary rocks (Stowe 1979; Nutt et al. 1988a; Campbell and Pitfield 1994). One of them passes the Ford mine about 500 m to the east. The TMDZ crosscuts the greenstone belt sequence NNW-SSE and joints the Munyati shear zone further north (Fig. 1). One splay passes the Ford mine 800 m to the west. The SDZ and TMDZ are interpreted as a shear couple with duplexing between the two zones (Campell and Pitfield 1994). Emplacement of the Ford granite is probably related to shearing between the two deformation zones.

Volcanic rocks within the Kwekwe district exhibit a subvertical bedding and foliation striking NNW-SSE and NNE-SSW. Isoclinal folding of the Bulawayan and Shamvaian greenstone successions and shear-zone development are the dominant styles of deformation and are related to an E-W compressional tectonic regime (Porter and Foster 1991; Buchholz 1995). Brittle faults, generally of WNW-ESE strike, displace the greenstone sequence particulary in the Broomstock and Jojo mine areas. They affected the craton probably in Proterozoic times as a result of extensional tectonis and generally are not favorable targets for gold exploration (Campbell and Pitfield 1994).

Geology of the Ford deposit

The country rocks in the area of the Ford mine comprise metabasalts, felsic volcanics (rhyolites), and BIFs of the Upper Bulawayan (Fig. 3). Tholeiitic metabasalts are pillowed in places and dip steeply. To the west of the ore body, porphyritic felsic volcanic rocks are intercalated and strike 500 m NNE-SSW with a maximum thickness of 150 m. Felsic agglomerates have been found in several places. Further to the west, strongly limonitized, steeply dipping and up to 4 m thick BIFs were found at the contact between the rhyolites and the metabasalts. They consist of alternating layers of chert and magnetite; three samples from a BIF outcrop ~20 m south of the granite dike contact carry up to 4 ppm Au. Approximately 1 km to the north of the open pit, in the Indarama mine area, ultramafic rocks of komatiitic affiliation and sulphide-bearing banded iron formations containing chalcopyrite, arsenopyrite, pyrrhotite, sphalerite, and magnetite are exposed (Buchholz et al. 1991). The vol-

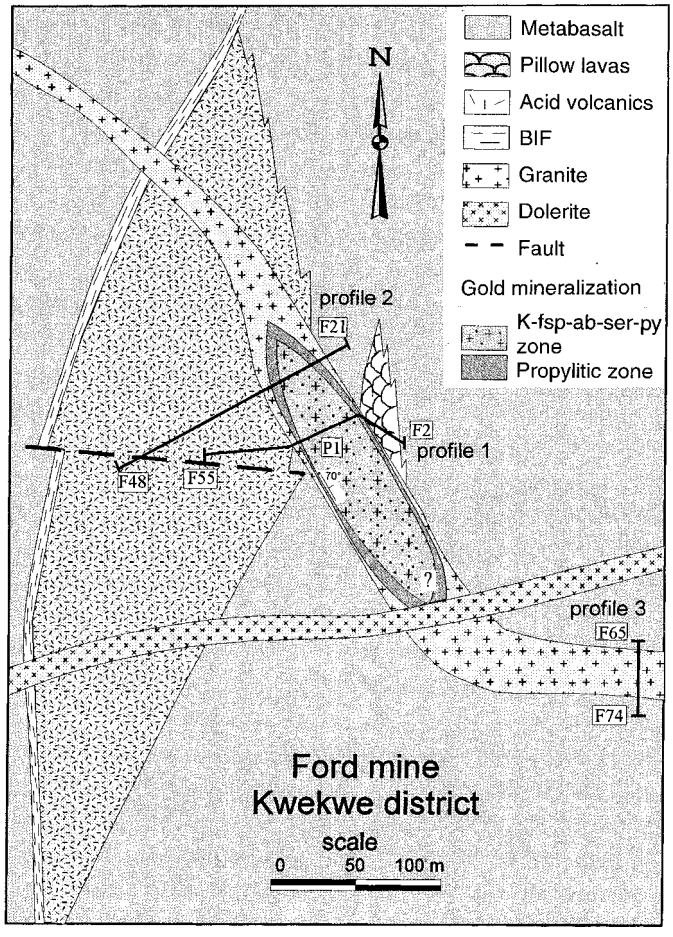

Fig. 3 Geological map of the Ford mine. The orebody is located within the s-shaped part of the granite dike dipping 70° to the NE. Gold mineralization occurs within the central K-feldspar-albite-sericite-pyrite zone and the marginal propylitic zone. The granite dike crosscuts a volcano-sedimentary sequence of the Upper Bulawayan Group

cano-sedimentary sequence at the Ford mine is intruded by a 20–50 m thick, sigmoid-shaped granite dike, which strikes NNW-SSE over a distance of more than 800 m and dips at 70° to the NE (Fig. 3). The southern flank of the dike almost turns into N-S direction as indicated on air photographs (see Fig. 2). A ~5 km long, E-W-striking dolerite dike crosscuts the entire sequence. The dolerite dike and a WNW-ESE striking brittle fault north of the dolerite dike (Fig. 3) are probably related to Proterozoic deformation and stabilization of the craton but are generally no indicators for gold mineralization. Detailed structural data of the deposit could not be obtained because outcrops during rediscovery in 1992 were limited to trenches; most of the open pit's bottom was covered by ore gravel in 1993 which made structural investigations almost impossible. However, several boulders within the open pit bear indications of shearing but orientation is obscure.

The unaltered parts of the granite dike are characterized by a white to gray, partly red color and a fine to medium grained matrix at the contact to the country rocks and a distinct porphyritic texture towards the center (Fig. 5, sample 1). The K-feldspar phenocrysts show a complex zoning. The albitic cores of large crys-

Fig. 4 View of the open pit of the Ford mine to the east

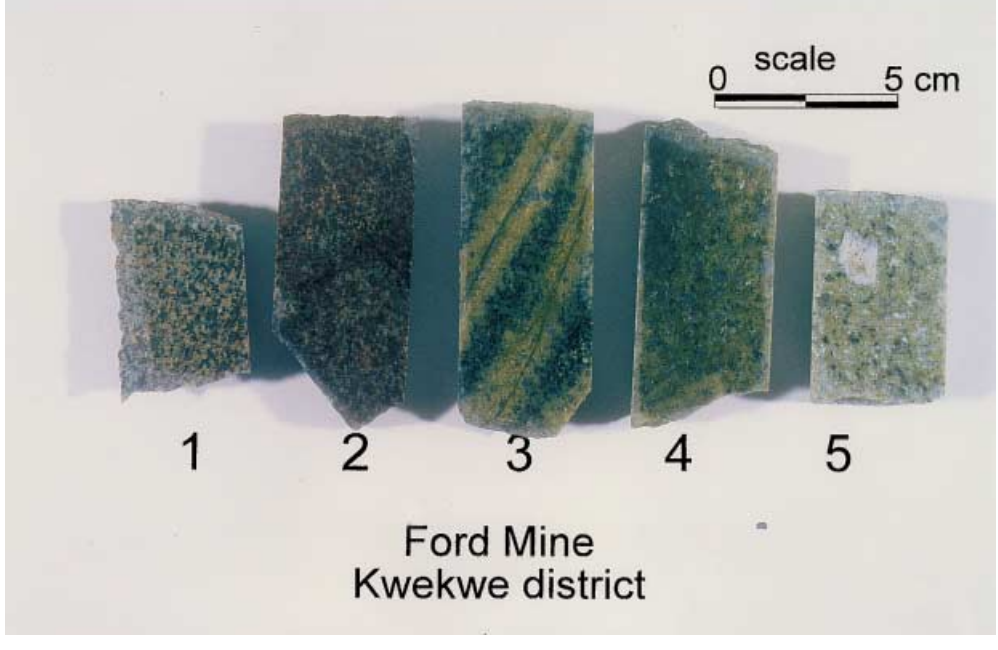

Fig. 5 Drill core samples from ~100 m depth of the Ford orebody. The drill core pieces have been sampled within ~1 m intervals from the hanging wall contact (*1*) of the granite dike to the altered and mineralized central zone (*5*). *1*, fine grained and unaltered gray, biotite-bearing granite; *2*, slighlty altered red granite; *3*, veinlets with green alteration halos crosscutting the granite, *4*, mineralized, dark greenish granite; *5*, strongly altered and mineralized greenish granite with alkali feldspar phenocryst

tals are dark-gray to red, whereas the rims consist of several white K-feldspar sub-zones, indicating continuous growth during cooling of the melt. Small inclusions of plagioclase and biotite are oriented along the growth zones. The size of porphyritic feldspar laths increases towards the center of the granite dike; the laths range from 2 cm up to 8 cm in size which probably is a function of cooling. The phenocrysts are embedded in a medium- to coarse-grained matrix. Albite is common in the matrix and partly sericitized. Xenomorphic plagioclase (andesine) shows typical albitic twinning lamellae (Fig. 6A). The total plagioclase content of the rock (with An > 5 %) is about ~10 vol.%. Hypidiomorphic, white perthitic K-feldspar in the matrix contains oligoclase inclusions. K-feldspar shows a typical dark and cloudy alteration under transmitted light (Fig. 6B). Myrmekitic textures between K-feldspar and quartz are rare. Biotite (~5 vol.%) forms aggregates up to 1.5 mm in size (altered biotite shown in Fig. 6C). Inclusions of leucoxene and rutile are oriented along the biotite cleavage planes. Quartz phenocrysts have a grain size of up to 5 mm and are strongly resorbed (Fig. 6D). Ilmenite, apatite, zircon, monazite, and xenotime are accessories. A paragenetic sequence of primary magmatic minerals in unaltered granite is given in Fig. 7. For classification of the rock unmineralized but weathered samples of profile 3 have been used and are compared with mineralized samples of profiles 1 and 2 (location of profiles shown in Fig. 3). Geochemical classification after Middlemost (1985) and de la Roche et al. (1980) (Fig. 8A,B), as well as microscopic studies show that the rock has a granitic composition. The low CaO content of the unmineralized rock probably resulted from weathering and may be misleading to classification. Metasomatic processes within the orebody redistributed major elements, but the primary major element content of the rock has probably not much changed during alteration (see later). Therefore, e.g., the CaO content of the mineralized samples point to the primary CaO content of the unmineralized rock (Fig. 8B). Mafic xenolithes of 5–50 cm in diameter occur within the granite dike. Those found in the open pit are mineralized and highly altered.

Alteration

Petrology

The country rocks at the Ford mine are altered within a narrow zone of 1–3 m thickness each side of the intrusion. In the SSW of the open pit, the footwall rhyolites are altered to cherty quartzitic rocks. At the hanging wall contact in the NNE, metabasalts are highly propylitized. Pyrite and gold are almost absent in the alteration zones surrounding the granite.

Within the orebody, alteration is pronounced and consists of a narrow, marginal propylitic zone and a central K-feldspar-albite-sericite-pyrite-zone. Based on unweathered drill core samples from a 100 m deep drill hole, alteration zonation over a distance of ~5 m is clearly shown. At the hanging wall contact, relatively fresh granite is medium to fine grained and biotite-rich (Fig. 5, sample 1). The degree of alteration of the granite increases towards the central zone. The color of the granite grades from gray to red (Fig. 5, sample 2) and green (Fig. 5, samples 3–5). Alteration within the propylitic zone proceeds along microshears and is indicated by its greenish color (Fig. 5, sample 3). Strongly altered and mineralized granite is characterized by the occurrence of disseminated pyrite (Fig. 5, sample 5). In profiles 1 and 2, the two alteration zones can be distinguished by differences in the degree of weathering. Rocks of the outer propylitic zone are highly weathered whereas rocks of the inner K-feldspar-albite-sericite-pyrite zone are almost resistant to weathering.

The propylitic zone is defined by chloritization and carbonate alteration of biotite (Figs. 6C and 7; Table 1, reaction 1), carbonate alteration of plagioclase, alteration of ilmenite to rutile (Fig. 9E; Table 1, reaction 2), and progressive sericitization of biotite, plagioclase and minor K-feldspar (Table 1, reactions 3, 4, and 5). Interstitial rutile/leucoxene and idiomorphic, fine-grained pyrite are abundant in chloritized biotite and as hypidiomorphic grains in the matrix. Idiomorphic white and reddish alkali feldspar crystals of up to 2 cm in diameter are partly sericitized.

The K-feldspar-albite-sericite-pyrite zone in profile 1 is 30–35 m thick and in profile 2 ~15–20 m (Fig. 2). The altered greenish rock is extremely hard. The green color is due to greenish sericite replacing mainly alkali feldspar (Fig. 6F,H). Its color is probably related to elevated Fe^{3+} in the sericite lattice (FeO_{total} content is up to 1.5 wt. %), as described by Wilcox (1987) and Rossmann (1987). Furthermore, the central zone is characterized by formation of secondary K-feldspar in the matrix (Fig. 6E), as detected by cathodoluminescence (CL) (see later), by albitization of plagioclase as detected by scanning electrone microscopy (SEM) studies, by carbonates, and by sericitization and carbonate alteration of biotite and chlorite, respectively (Fig. 6G). The alteration pattern indicates metasomatic reactions during ore formation. K^+, Na^+, and Ca^{2+} primarily bound in feldspars have been remobilized during fluid-rock interaction and sericitization (Table 1, reactions 4 and 5). K^+ has been consumed during formation of secondary K-feldspar, which probably postdates sericitization (Table 1, reaction 6), Na^+ during albitization of oligoclase/andesine (Table 1, reaction 7), and Ca^{2+} during carbonate formation (Table 1, reaction 8). SiO_2 (H_4SiO_4) liberated during sericitization has probably entirely be consumed during albitization of plagioclase and secondary K-feldspar formation because secondary quartz has not been detected (see CL investigations later). Fe^{2+} liberated from altered ilmenite and biotite has been consumed during pyrite formation (Table 1, reactions 2 and 3). Mg^{2+}, which has been liberated from altered biotite as well, might have been bound in Mg-

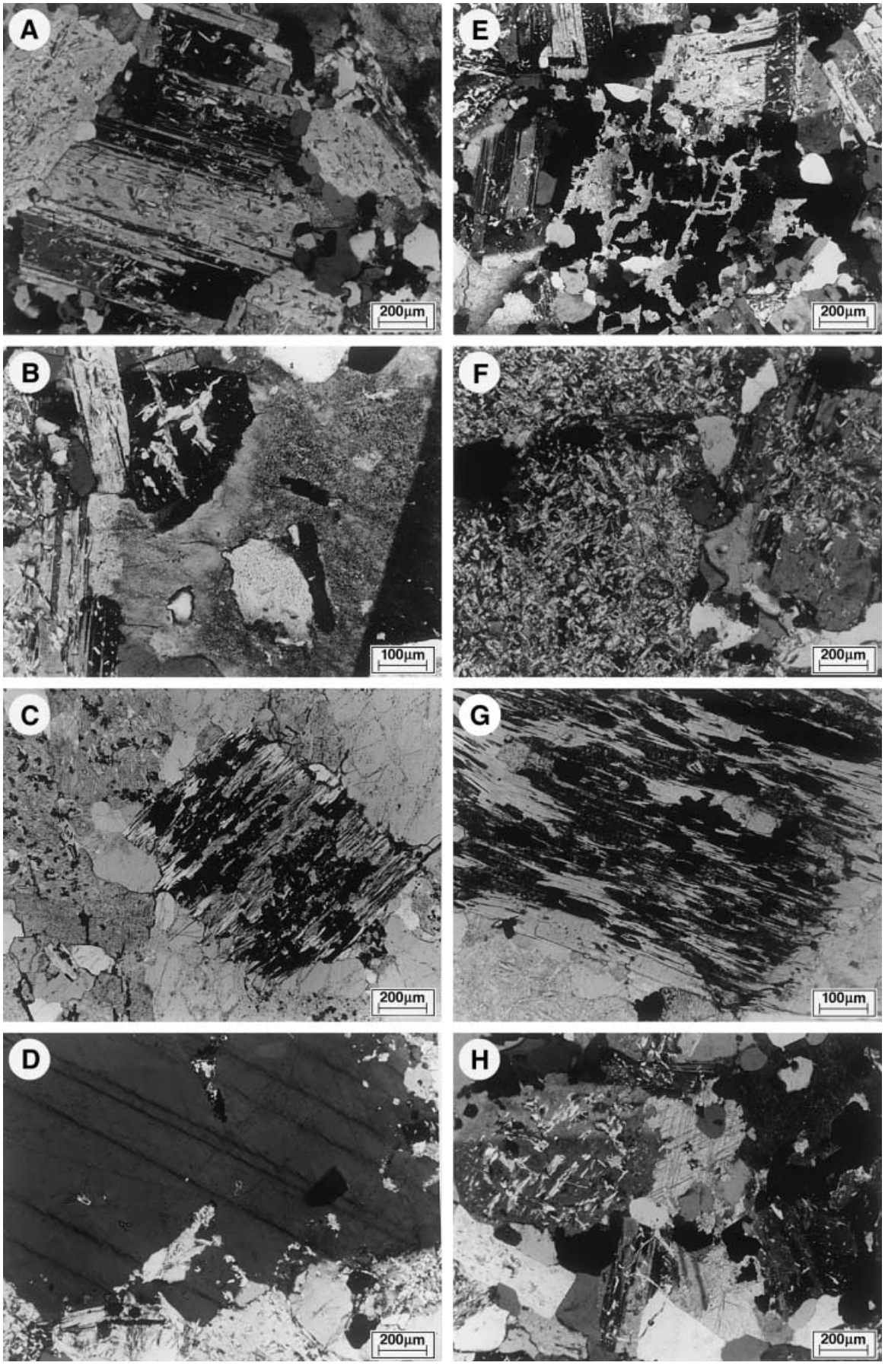
A
200μm
E
200μm
B
100μm
F
200μm
C
200μm
G
100μm
D
200μm
H
200μm

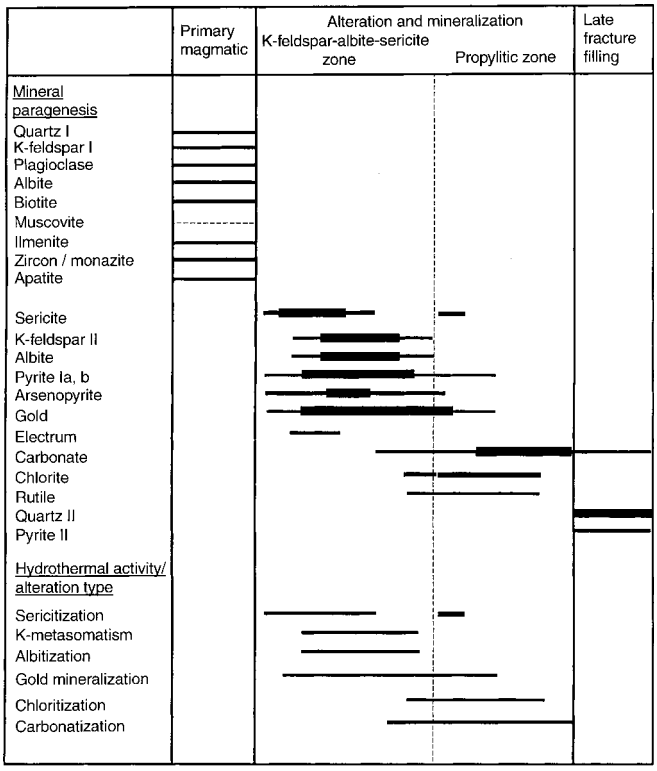

Fig. 7 Primary mineralogy of the Ford granite dike and paragenetic sequence for the gold-bearing K-feldspar-albite-sericite-pyrite and propylitic zones

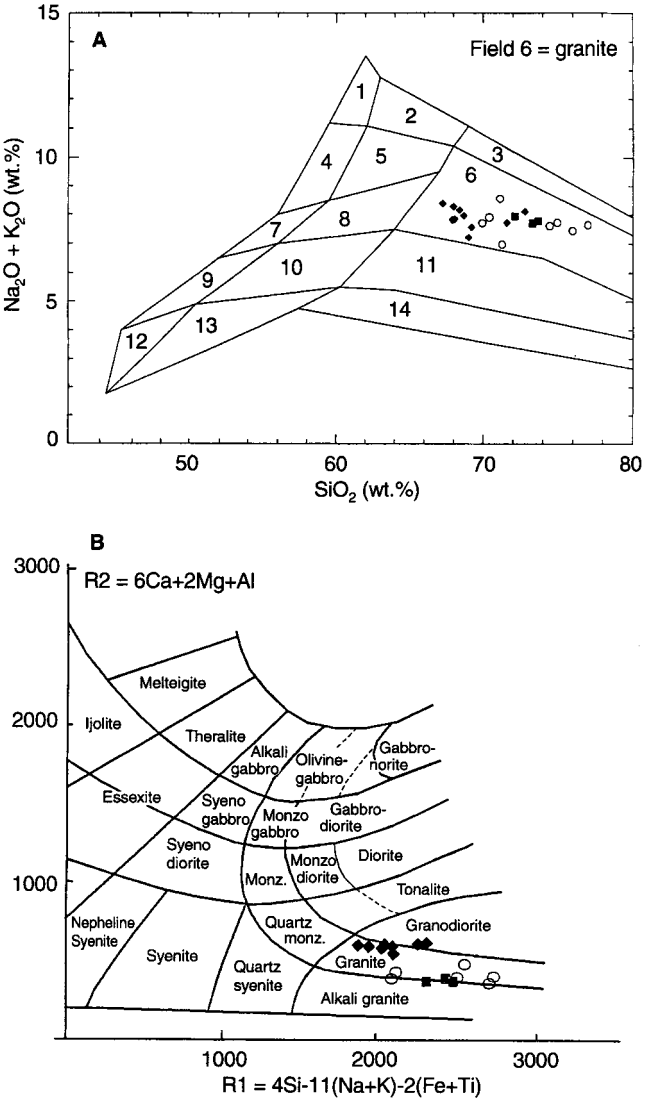

Fig. 8A, B Classification diagrams after **A** Middlemost (1985) and **B** De la Roche et al. (1980) with position of mineralized and unmineralized samples of the Ford granite. (*circles*, unmineralized samples of profile 3 and samples F 7, 17, 29 of profiles 1 and 2; *boxes*, mineralized samples from the propylitic zone of profiles 1 and 2; *diamonds*, mineralized samples from the K-feldspar-albite-sericite-pyrite zone of profiles 1 and 2; fields in **A**: *1*, alkali feldspar syenite, *2*, alkali feldspar quartz syenite; *3*, alkali feldspar granite; *4*, syenite, *5*, quartz syenite; *6*, granite; *7*, monzonite; *8*, quartz monzonite; *9*, monzodiorite; *10*, quartz monzodiorite; *11*, granodiorite; *12*, diorite and gabbro; *13*, quartz diorite; *14*, tonalite)

biotite (phlogopite). Relicts of less carbonate altered, chloritized dark mica are locally abundant in the K-feldspar-albite-sericite-pyrite zone which may indicate that a second generation of dark mica was formed during alteration. H_2O, H_2S, HCO_3^- (CO_2), must have been added during alteration. At the beginning of alteration, the pH of the fluid was probably acidic (chloritization, sericitization, secondary K-feldspar formation) and changed later to alkalic (carbonate formation) conditions. Gold probably precipitated during oxidation of sulphur and pyrite formation (Table 1, reactions 2 and 3).

Quartz phenocrysts of 3–5 mm size show deformation bands with preferred orientation as well as recrystallization textures (Fig. 6D). The occurrence of deformation bands is conformable with the observation of an orientated rock fabric found in some mineralized boulders in the open pit. Pyrite and minor arsenopyrite are disseminated and form aggregates of up to 6 mm in size. The extreme toughness of rocks from the K-feldspar-albite-sericite-pyrite zone for crushing and its high

◀

Fig. 6A–H Thin sections of mineralized granite samples from the central K-feldspar-albite-sericite-pyrite and the marginal propylitic zone of the Ford mine. **A** partly sericitized and albitized plagioclase (extinction 20°) with alkali feldspar and quartz of the central zone (sample F 13, 22920, crossed nicols); **B** altered K-feldspar I with plagioclase and quartz of the central zone (sample F 13, 22920, crossed nicols); **C** chloritized biotite of the porpylitic zone (sample F 7, 22890, plane polarized light); **D** quartz phenocryst with deformation bands due to tectonic overprint of the mineralized granite (sample F 12, 22890, crossed nicols); **E** secondary carbonate and K-feldspar II (black) with plagioclase and quartz of the central zone (sample F 9, 22891, crossed nicols); **F** strongly sericitized alkali-feldspar and partly sericitized plagioclase of the central zone. Sericite is characterized by a greenish color (sample F 12, 22892, crossed nicols); **G** carbonatized and sericitized biotite with pyrite Ib and rutile on cleavage planes, central zone (sample F 13, 22920, plane polarized light); **H** pyrite grains (black) with carbonate and sericitized plagioclase and albite of the central zone (sample F 91, 22898, crossed nicols)

Table 1 Alteration processes and chemical reactions within the mineralized granite at the Ford gold deposit (for explanation see text)

Alteration processes and chemical reactions
1. Chloritization of biotite $2KMg_3AlSi_3O_{10}(OH)_2 + 4H^+ \Longleftrightarrow Mg_5Al_2Si_3O_{10}(OH)_8 + 3SiO_2 + 2K^+ + Mg^{II+}$
2. Alteration of ilmenite to rutile (leukoxen) $FeTiO_3 + 2Au(HS)_2^- \Longleftrightarrow FeS_2 + 2\,Au^\circ + 2\,HS^- + TiO_2 + H_2O$
3. Sericitization of biotite and formation of pyrite $K(Mg,Fe^{II+})_3[(OH,F)_2/AlSi_3O_{10}] + 2Al^{III+} + 2Au(HS)_2^- \Longleftrightarrow KAl_2[(OH,F)_2/AlSi_3O_{10}] + Mg^{II+} + 2FeS_2 + 2\,Au^\circ + 4H^+$
4. Sericitization of K-feldspar $3KAlSi_3O_8 + 2H^+ + 12H_2O \Longleftrightarrow KAl_2[(OH)_2/AlSi_3O_{10}] + 2K^+ + 6H_4SiO_4$
5. Sericitization of plagioclase $3NaAlSi_3O_8 + K^+ + 2H^+ + 12\,H_2O \Longleftrightarrow KAl_2[(OH)_2/AlSi_3O_{10}] + 3\,Na^+ + 6H_4SiO_4$ $3CaAl_2Si_2O_8 + 2K^+ + 4H^+ \Longleftrightarrow 2KAl_2[(OH)_2/AlSi_3O_{10}] + 3Ca^{II+}$
6. Secondary K-feldspar formation $K^+ + 3H_4SiO_4 + Al^{III+} \Longleftrightarrow KAlSi_3O_8 + 4H_2O + 4H^+$
7. Albitization of plagioclase $CaAl_2Si_2O_8 + 2Na^+ + 4H_4SiO_4 \Longleftrightarrow 2NaAlSi_3O_8 + Ca^{II+} + 8H_2O$
8. Carbonate formation $Ca^{II+} + 2HCO_3^- \Longleftrightarrow CaCO_3 + H_2O + CO_2$

resistance to weathering is probably a result of strong sericitization and formation of secondary K-feldspar. The mafic xenolithes within the mineralized granite are characterized by chlorite alteration and carry large quantities of pyrite. High pyrite contents indicate that the elevated primary Fe-content of the xenolithes favored pyrite precipitation.

The transition of the propylitic zone and the K-feldspar-albite-sericite-pyrite zone is gradational (e.g., Fig. 5, samples 3 to 5). Critical minerals do not occur; instead, the transition zone is characterized by an increase in biotite alteration (chlorite, pyrite, and sericite formation), ilmenite, plagioclase, and K-feldspar alteration, and minor addition of pyrite, carbonate, and secondary K-feldspar in the matrix.

CL investigations were carried out on mineralized granite slabs of the K-feldspar-albite-sericite-pyrite zone (14–15 kV, 0.6–0.8 mA, AO 54 Kathode, Agor Scientific Ltd.). They show that (1) hydrothermal quartz with a typical short-lived blue luminescence is absent, and (2) secondary, unaltered K-feldspar with a light blue color occurs in the matrix together with carbonate, adjacent to pyrite, or as inclusions in pyrite aggregates (see Fig. 9H). Calcite has a deep orange color; its abundance increases towards the center of the intrusion. Calcite coatings around sulphide grains indicate its late paragenetic position. Primary K-feldspar generally shows a grey-purple to dark-blue luminescence due to strong sericitization. Greenish zones of albite occur within large K-feldspar phenocrysts. Apatite forms up to 1 mm-long crystals and appears zoned under CL. Porphyritic, corroded quartz phenocrysts and matrix quartz have a purple luminescence indicative of their magmatic origin (Marshall 1987; Götze 1994). In a few cases, porphyritic quartz phenocrysts are zoned, a feature typically observed in subvolcanic and extrusive rocks (Götze, personal communication 1996).

Geochemistry

Forty-six samples of hydrothermally altered (profiles 1 and 2, Fig. 3) and unaltered (profile 3, Fig. 3) granite, metabasalt, and felsic volcanics were analyzed for major and trace elements (Table 2). Mass balance calculations after Gresens (1967) using this data set do not seem appropriate, because mining remains active within the weathered part of the orebody. In particular, hydrothermally unaltered granite samples and ore samples of the propylitic zone are affected by weathering. The number of drill core samples was not sufficient for geochemical characterization of the orebody from deeper sections.

However, comparison of the absolute data of profile 3 with profiles 1 and 2 shows that (1) only small element variations occur in unmineralized granite of profile 3, and (2) Au, As, P_2O_5, CaO, MgO, and partially Ba, and Sr are elevated within the mineralized granite (Figs. 10, 11). Moderate to considerable variations are evident for Al_2O_3, SiO_2, Na_2O, K_2O, and Rb, small variations are indicated for TiO_2, Fe_2O_3, MnO, Pb, Sb, Y, and Zr.

►

Fig. 9A–H Polished sections of gold and sulphide-bearing granite samples of the Ford mine. **A** pyrite Ia with Au-grains (*arrow*) (sample FS 1, 25642, plane polarized light); **B** gold grains within secondary K-feldspar I (detailed section of **A**, sample FS 1, 25642, plane polarized light); **C** pyrite Ia with gold (*arrow*) (sample N 3, 22919, plane polarized light); **D** gold in pyrite Ia (*arrow*) (detailed section of **C**, sample N 3, 22919, plane polarized light); **E** ilmenite laths replaced by rutile and pyrite (sample FS 1, 25642, plane polarized light); **F** altered biotite with pyrite Ib and rutile on cleavage planes (sample FS 1, 25642, plane polarized light); **G** pyrite Ia with irregular grain boundaries within a mineralized and chloritized mafic xenolithe (sample F 44, 22900, plane polarized light); **H** idiomorphic pyrite IIa with rounded quartz and secondary K-feldspar (sample F 64, 22904, plane polarized light)

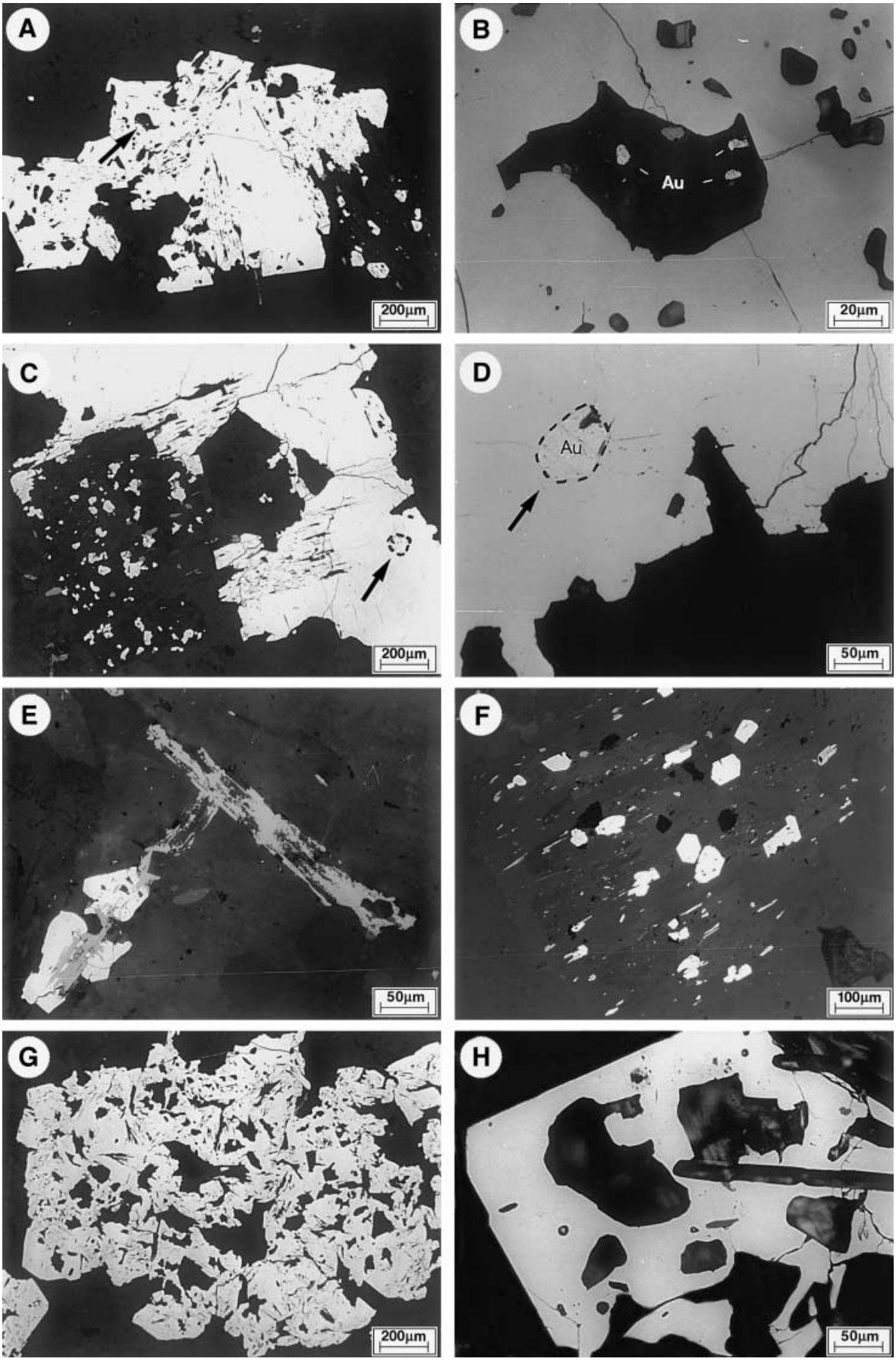
A
200μm
B
Au
20μm
C
200μm
D
Au
50μm
E
50μm
F
100μm
G
200μm
H
50μm

Table 2 Chemical analyses of major and trace elements from profiles 1, 2, and 3 of the Ford gold deposit (M, metabasalt; *G*, granite; fV, felsic volcanics; – below detection limit, D.L., detection limit; n.a, not analyzed)

Profile 1	Host rock					Propylitic zone		K-fsp-ab-ser-py zone				Propylitic zone		Host rock					Profile 2		Host rock		D.L.
	F2 M	F3 M	F4 M	F5 M	F6 M	F7 G	F8 G	F9 G	F10 G	F11 G	F13 G	F14 G	F15 G	F17 G/fV	F19 fv	F20 fv	F53 fv	F55 fv	F21 M	F24 M	F25 M	F28 M/G	
wt.%																							
SiO_2	56.84	51.69	57.33	61.52	72.17	69.95	68.42	68.71	68.02	67.93	67.27	71.13	69.02	73.89	73.73	73.53	75.36	73.27	51.49	55.85	69.95	54.11	0.02
TiO_2	0.72	0.88	0.96	0.71	0.47	0.37	0.33	0.33	0.32	0.35	0.33	0.34	0.33	0.38	0.25	0.23	0.27	0.24	0.99	1.07	1.26	1.20	0.01
Al_2O_3	16.94	17.53	15.77	15.22	15.94	16.25	14.67	14.24	14.52	14.95	14.96	15.69	14.47	14.86	16.09	14.02	16.58	16.32	15.52	15.89	18.69	17.15	0.20
Fe_2O_3	6.74	5.63	6.11	4.66	2.69	2.29	2.02	1.84	1.89	1.87	1.77	2.08	1.99	1.45	0.88	0.45	0.26	0.90	8.89	8.04	1.74	10.34	0.01
MnO	0.08	0.11	0.10	0.08	0.01	0.02	0.01	0.01	0.02	0.02	0.02	0.01	0.01	0.05	–	–	–	0.01	0.19	0.22	0.01	0.18	0.01
MgO	1.59	4.47	4.37	3.12	0.40	0.23	0.72	0.69	0.69	0.73	0.56	–	0.66	0.37	0.48	0.68	0.44	0.93	5.36	5.84	1.79	5.38	0.20
CaO	16.65	13.39	10.58	6.56	0.24	0.39	2.26	2.25	2.43	2.38	2.30	0.32	2.25	0.32	0.65	0.93	0.06	0.07	10.66	9.82	0.13	5.10	0.02
Na_2O	–	1.60	1.62	3.30	3.32	5.65	4.78	4.63	5.03	4.77	4.96	5.06	4.66	4.95	5.71	3.55	0.47	–	2.42	2.71	0.54	3.14	0.30
K_2O	–	1.24	0.61	0.96	3.06	2.06	3.38	3.34	3.26	3.05	3.43	3.51	2.56	2.00	1.99	2.26	3.99	4.61	0.85	0.20	2.00	0.48	0.05
P_2O_5	0.06	0.07	0.10	0.14	0.05	0.12	0.13	0.13	0.13	0.14	0.13	0.13	0.14	0.08	0.05	0.02	0.03	–	0.08	0.09	0.06	0.09	0.02
V_2O_5	0.04	0.01	0.05	0.02	0.01	0.01	–	–	0.01	0.01	0.01	0.01	0.01	0.01	0.01	–	–	–	0.05	0.05	0.05	0.06	0.005
Cr_2O_3	0.04	0.06	0.05	0.03	–	–	–	–	–	–	–	–	–	–	–	–	–	–	0.04	0.04	0.05	0.05	0.005
SO_3	–	–	–	–	–	–	–	–	–	–	–	–	–	–	–	–	–	–	–	–	–	–	5.00
LOl	1.80	2.60	1.60	2.47	1.99	1.39	2.91	2.84	2.92	3.52	2.70	1.15	2.60	1.35	1.18	1.63	2.28	2.63	2.51	0.78	2.35	1.58	
Total	101.76	99.37	99.30	99.16	100.39	98.72	100.25	99.58	99.95	99.95	99.12	99.54	98.95	99.69	101.02	97.35	99.74	99.20	99.10	100.59	96.61	98.85	
ppm																							
Au	0.4	0.4	–	0.4	1.2	1.2	1.2	6.0	1.2	3.2	7.2	1.6	2.0	0.4	0.4	0.8	n.a.	n.a.	0.4	–	–	0.4	0.4
Bi	–	–	–	–	–	–	–	–	–	–	–	–	–	–	–	–	–	–	–	–	–	–	20
Pb	–	–	–	–	12	20	19	20	19	31	20	18	19	15	18	10	61	10	–	–	–	–	10
Sb	–	–	–	–	37	18	–	–	–	–	–	–	–	–	–	–	–	–	–	–	20	–	20
As	34	10	11	129	1292	976	129	295	62	600	73	256	25	73	34	29	12	10	–	–	20	60	10
Ba	94	117	311	526	782	661	1154	1069	1118	1044	1116	1159	941	793	507	399	430	641	135	235	295	704	50
Mo	–	–	–	–	–	–	–	–	–	–	–	–	–	–	–	–	–	–	–	–	–	–	10
Nb	–	–	–	–	–	–	–	–	–	–	–	–	–	–	–	–	–	–	–	–	–	–	10
Zr	53	63	70	120	174	166	145	140	141	139	138	143	139	158	125	119	138	132	73	79	88	82	20
Y	18	17	22	15	12	–	–	–	–	–	–	–	–	–	–	–	10	–	21	22	19	34	10
Sr	73	78	87	382	187	325	571	538	528	517	480	377	558	296	242	85	43	14	127	146	19	155	10
Rb	–	67	33	38	104	72	101	104	104	98	104	99	67	72	56	58	78	109	45	–	51	22	10
Ga	25	18	18	17	21	21	19	19	20	20	20	20	20	18	19	17	20	17	19	18	19	14	10
Zn	28	108	76	54	–	18	20	25	–	19	–	18	35	19	26	18	38	–	84	97	242	117	20
Ni	94	130	131	64	–	–	–	–	–	–	–	–	–	–	–	–	–	–	96	82	151	154	20
Co	26	33	45	27	–	–	–	–	–	–	–	–	–	–	–	–	–	–	38	34	12	49	20
Cu	52	22	90	83	69	–	–	–	–	–	–	–	–	–	–	–	–	–	74	86	36	118	20
Cd	–	–	–	–	–	–	–	–	–	–	–	–	–	–	–	–	–	–	–	–	–	–	20

Table 2 (Contd.)

Profile 2	Propylitic zone				K-fsp-ab-ser-py zone				Propylitic zone		Host rock			Profile 3										D.L.
	F 29 G	F 30 G	F 32 G	F 33 G	F 35 G	F 37 G	F 38 G	F 40 G	F 41 G	F 42 G	F 46 G/SV	F 47 SV	F 48 SV	F 65 M	F 66 M	F 67 M	F 68 M/G	F 69 G	F 70 G	F 71 G	F 72 G/M	F 73 M	F 74 M	
wt.%																								
SiO_2	55.85	74.97	71.26	71.60	72.80	69.22	68.09	76.00	74.45	69.54	70.40	75.37	75.48	56.05	59.29	56.04	71.80	72.13	73.32	73.69	70.92	90.99	74.73	0.02
TiO_2	1.07	0.37	0.34	0.34	0.33	0.34	0.34	0.35	0.35	0.39	0.35	0.24	0.23	1.19	1.01	1.01	0.36	0.37	0.40	0.37	0.38	0.01	1.07	0.01
Al_2O_3	15.89	16.75	15.23	14.98	15.23	14.39	14.75	15.00	15.23	15.41	14.84	14.45	14.30	17.96	16.53	15.70	16.15	15.96	16.10	15.90	17.00	0.17	16.34	0.20
Fe_2O_3	8.04	2.17	2.15	1.82	2.14	1.93	2.29	1.93	2.34	2.12	2.19	0.57	0.89	5.80	5.50	9.36	2.27	2.10	2.10	2.13	2.52	9.01	2.37	0.01
MnO	0.22	–	0.03	0.01	0.04	0.01	0.01	0.01	0.02	0.03	0.01	0.03	0.03	0.10	0.11	0.10	0.02	0.01	0.04	0.02	0.02	0.05	0.02	0.01
MgO	5.84	0.35	0.25	0.23	0.22	0.66	0.73	0.28	0.29	0.74	0.83	0.34	0.60	2.72	3.25	1.27	0.21	–	0.25	0.30	0.43	–	0.48	0.20
CaO	9.82	0.15	1.08	1.46	0.34	2.27	2.27	0.39	0.33	2.18	2.32	1.49	0.10	12.42	9.04	14.55	0.16	0.14	0.11	0.15	0.28	0.06	0.48	0.02
Na_2O	2.71	5.18	4.15	4.78	5.24	4.48	4.84	4.52	5.07	4.68	5.11	3.55	1.25	0.75	3.26	0.09	4.48	4.71	4.72	4.54	4.00	–	0.58	0.30
K_2O	0.20	2.55	5.83	2.94	2.87	3.09	3.01	2.94	2.55	2.00	2.11	1.97	3.99	0.07	0.78	–	3.39	3.23	2.96	3.24	2.83	–	0.97	0.05
P_2O_5	0.09	0.02	0.14	0.15	0.11	0.13	0.13	0.14	0.13	0.13	0.15	0.05	0.05	0.04	0.06	0.05	0.02	0.04	–	–	0.02	–	0.05	0.02
V_2O_5	0.05	0.01	–	–	0.01	–	0.01	–	0.01	–	0.01	–	–	0.05	0.04	0.05	0.01	0.01	0.01	0.01	0.01	–	0.04	0.005
Cr_2O_3	0.04	–	–	–	–	–	–	–	–	–	–	–	–	0.05	0.04	0.05	–	–	–	–	–	–	0.04	0.005
SO_3	–	–	–	–	–	–	–	–	–	–	–	–	–	–	–	–	–	–	–	–	–	–	–	5.00
LOl	1.49	1.18	1.86	1.97	1.23	2.96	3.16	1.40	1.46	2.22	1.63	1.55	2.23	3.31	2.07	2.47	1.69	1.56	1.66	1.67	3.11	0.84	1.24	
Total	101.30	103.69	99.45	100.33	100.53	100.10	100.21	102.95	102.21	99.44	100.40	99.60	99.15	100.49	101.02	100.75	100.57	100.46	101.70	102.01	101.61	101.21	98.42	
ppm																								
Au	0.4	3.2	2.0	2.4	2.8	1.6	2.8	1.2	4.0	n.a.	1.6	0.4	1.6	–	–	0.40	–	–	–	–	0.40	0.40	0.40	0.4
Bi	–	–	–	–	–	–	–	–	–	–	–	–	–	–	–	–	–	–	–	–	–	–	–	20
Pb	12	21	26	22	18	18	17	16	24	16	21	14	–	11	–	–	23	21	22	21	24	–	262	10
Sb	–	–	–	–	–	–	–	–	–	–	–	–	–	–	–	–	–	–	–	–	18	–	29	20
As	149	695	1096	89	455	75	515	42	171	20	38	–	12	12	–	13	20	41	29	22	26	15	160	10
Ba	864	1666	878	1125	1190	1141	1164	926	951	1025	1172	530	426	326	1192	226	1235	1271	1154	1265	1086	117	190	50
Mo	–	–	–	–	–	–	–	–	–	–	–	–	–	–	–	–	–	–	–	–	–	11	–	10
Nb	–	–	–	–	–	–	–	–	–	–	–	–	–	–	–	–	–	–	–	–	–	–	–	10
Zr	150	146	142	145	144	140	144	143	144	145	155	120	117	82	74	74	155	152	175	152	149	–	77	20
Y	–	–	–	–	–	–	–	–	–	–	–	–	–	12	19	13	–	–	–	–	–	–	26	10
Sr	356	387	278	379	400	529	580	383	363	620	371	98	19	135	152	428	370	389	361	386	387	–	19	10
Rb	81	99	88	84	89	87	92	80	76	67	82	43	86	–	42	–	95	90	92	90	81	–	32	10
Ga	20	20	21	20	20	18	19	19	20	20	20	16	16	23	17	32	20	22	20	20	21	–	–	10
Zn	–	20	26	–	24	22	20	–	27	23	21	21	–	67	59	23	26	23	28	23	25	–	513	20
Ni	–	–	–	–	–	–	–	–	–	–	–	–	–	156	100	64	–	–	–	–	–	–	144	20
Co	–	–	–	–	–	–	–	–	–	–	–	–	–	40	35	29	–	–	–	–	88	–	30	20
Cu	–	–	–	–	–	–	–	–	–	–	–	–	–	81	85	95	–	–	–	–	–	138	40	20
Cd	–	–	–	–	–	–	–	–	–	–	–	–	–	–	–	–	–	–	–	–	–	–	–	20

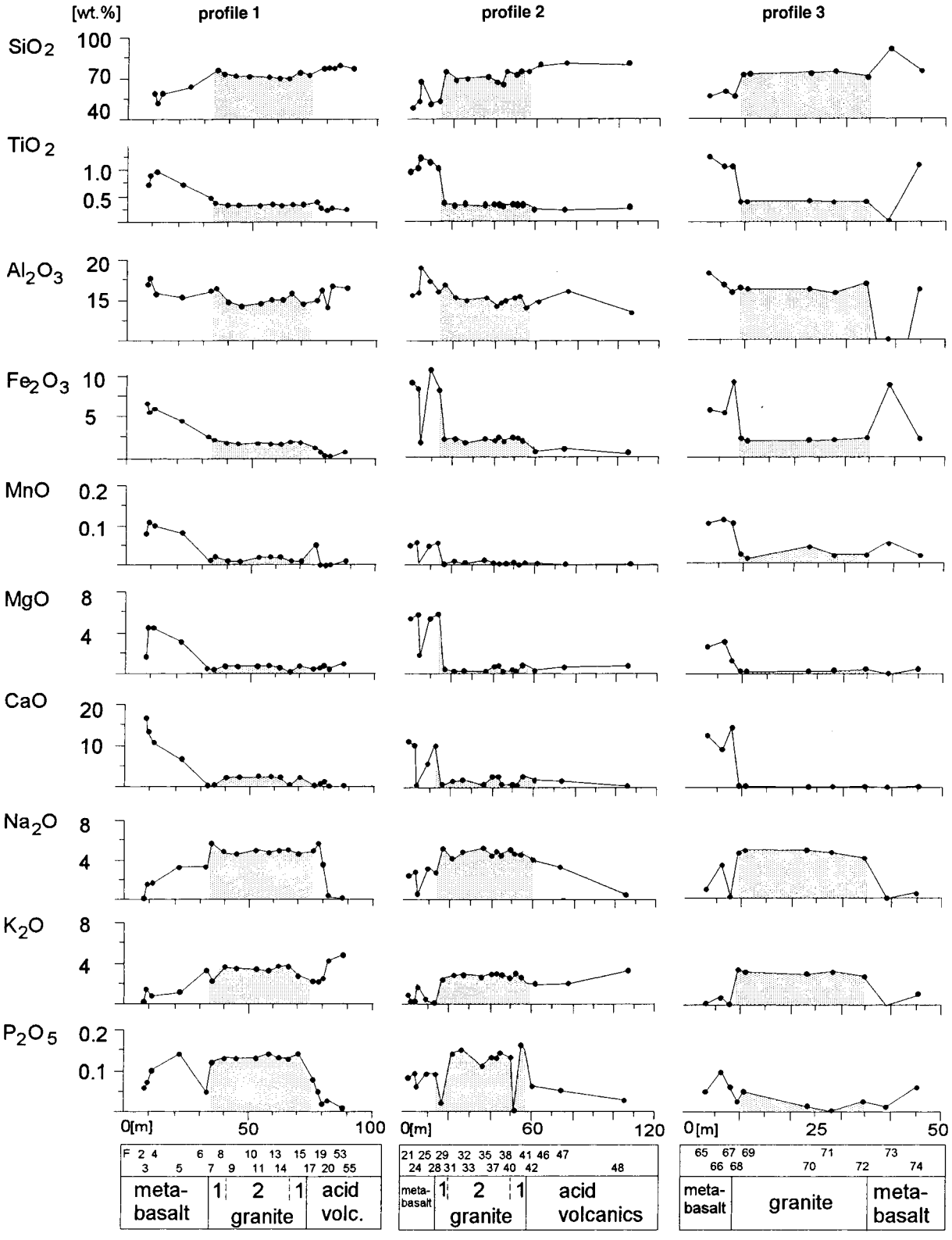

Fig. 10 Major element distribution of selected elements for the mineralized (*profiles 1 and 2*) and barren (*profile 3*) granite of the Ford mine as well as for host rocks (see Fig. 3 for location; *F 2–74*, sample numbers; *1*, propylitic zone; *2*, K-feldspar-albite-sericite-pyrite zone). Relative positions of samples indicated above the rock units

Au and As are clearly added and elevated values agree with the occurrence of native Au, electrum, probably invisible Au in pyrite, and arsenopyrite (see later) (average = 2.6 ppm, n = 35; As up to 1096 ppm, sample F 32, Table 2). The highest gold value measured is 18.7 ppm (not shown). P_2O_5, CaO, and MgO are

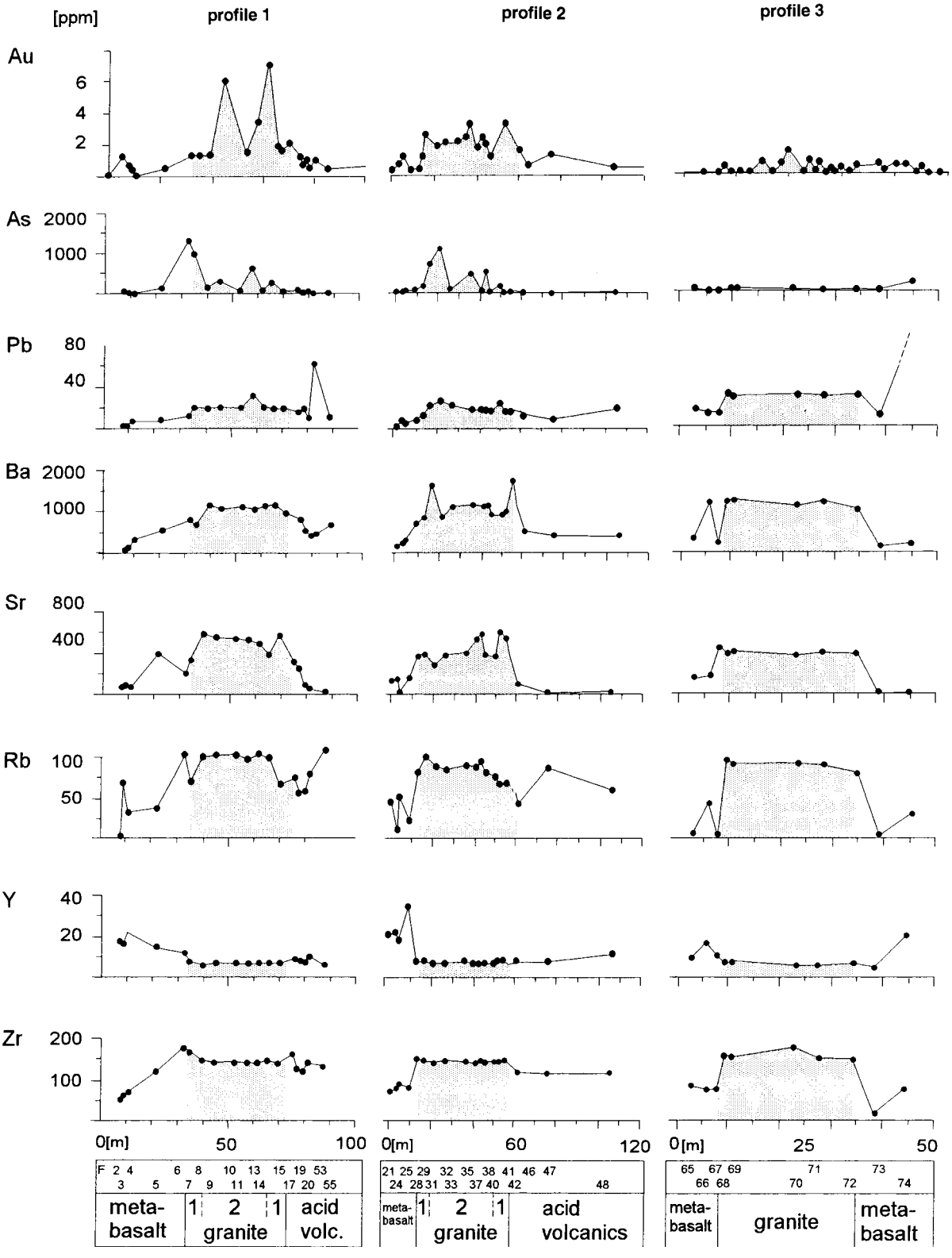

elevated in the mineralized granite and bound in apatite, carbonates, and (secondary?) biotite, respectively. They probably have been depleted in profile 3 because of weathering. Elevated values for Pb (31 ppm, sample F 11) and Sb (18 ppm, sample F 7) have been detected locally (Table 2).

Fig. 11 Trace element distribution of selected elements for the mineralized (*profiles 1 and 2*) and barren (*profile 3*) granite of the Ford mine as well as for host rocks (see Fig. 3 for location; *F 2-74*, sample numbers; *1*, propylitic zone; *2*, K-feldspar-albite-sericite-pyrite zone). Relative positions of samples indicated above the rock units

Geochemical distinction between the inner K-feldspar-albite-sericite-pyrite zone and the outer propylitic zone is generally not possible from this data. However, two distinct gold peaks in profile 1 (samples F 9 and 13) and profile 2 (samples F 31 and 41) occur in the transition zone. Additionally, two barium peaks in profile 2 (Fig. 11) and decrease of K_2O in the propylitic zone of profile 1 are obvious (Fig. 10 and Table 2).

Alterations within the host rocks of the intrusion along profiles 1 and 2 are pronounced compared to profile 3, but the alteration zone is only 3–5 m wide (effective distance of metabasalt samples to granite dike contact is 8–10 m, see Fig. 3). The large input of Na, K, and As, and minor inputs of Sr and Rb at the immediate contact of the mineralized granite with the metabasalts and felsic volcanics, respectively, attests to the direct influence of hydrothermal alteration on the host rocks. Alteration of the metabasalts (Na-K-As) along profile 3 is not observed, suggesting that the granite was relatively dry in nature at the time of intrusion and alteration has no direct relationship with dike emplacement. In the southern part of profile 3, one metabasalt sample (F 73) is cut by a quartz vein with elevated Cu contents (Table 2). Elevated Pb, Sb, As, and Zn values in sample F 74 are obvious, but the anomalous values are probably not related to the granite dike emplacement.

Gold and associated sulphide mineralization

Ore mineralogy

Pyrite has a grain size of 0.1–2 mm (type Ia, Figs. 7, 9A) and is restricted to the K-feldspar-albite-sericite-pyrite and the propylitic zones (Fig. 3). Its modal abundance is ~2–3 vol.%. The pyrite aggregates are hypidiomorphic to xenomorphic and commonly contain rounded grains of secondary K-feldspar (Fig. 9B,H), gold (Fig. 9B–D), and quartz (Fig. 9H), as well as aggregates of sericite, carbonate, and apatite. Mafic xenolithes within the granite are enriched in pyrite Ia due to their high Fe content. The shape of the pyrite grains differ from that within the mineralized granite due to intergrowth with chlorite (Fig. 9G). The chlorite grains within pyrite have been used for chlorite geothermometry (see later). Pyrite Ib is idiomorphic (15–100 μm size), but not distinct geochemically from pyrite Ia (n = 40 grains, 120 electron microprobe analyses). The pyrite Ib grains predominantly occur within cleavage planes of altered biotite (Fig. 9C, F). Idiomorphic to hypidiomorphic pyrite II is confined to 1–2 mm thick quartz-carbonate-filled linear fractures within the granite interpreted as cooling fractures.

Visible gold is rare and only a few gold grains have been found in 20 thin and polished sections. It occurs as round blebs of 5–10 μm size within pyrite Ia and K-feldspar (II) (Fig. 9A–D). One gold grain (100 μm in size) is highly porous and rimmed by electrum and by a second generation of gold with a filigree texture (not shown). Arsenopyrite is a minor component of the ore and occurs as idiomorphic crystals (up to 400 μm in size) within the altered granite or intergrown with pyrite Ia.

Geochemistry of gold and sulphide mineral separates

The average fineness of gold is 93.4 wt.% with a silver content of 5.7 wt.% (Table 3). The mercury content is ~0.3 wt.%. The silver content of one electrum grain is 26–39 wt.%. Neutron activation analyses of sulphide mineral separates give gold concentrations of 40–126 ppm. Because of the low abundance of native gold grains in the ore, it is suggested that the bulk of the gold occurs as submicroscopic inclusions in pyrite or in the pyrite lattice. The low silver and mercury contents of the separates compare to the low abundance of electrum and low contents in native gold. Single pyrite grains contain up to 1.3 wt.% As and generally < 0.02 wt.% Co and Ni (Table 3). The arsenic content of the sulphide separate is relatively low, comparable to the low abundance of arsenopyrite within the ore. The arsenic content within arsenopyrite varies between 26.2 and 33.4 atomic %, but

Table 3 Chemical analyses of gold and sulphides from the Ford gold deposit (EPMA data, electron-microprobe data; INAA, instrumental neutron activation analysis; X, average; SD, standard deviation; n.a, not analyzed; – below detection limit; D.L, detection limit)

		Au	Fe	As	S	Co	Cu	Ni	Zn	Sb	Ag	Hg	Te	Total
EPMA data [wt. %]														
Gold	×	93.43	0.14	–	n.a.	n.a.	–	n.a.	n.a.	–	5.68	0.32	–	99.87
n = 14	SD	1.33	0.38	–	n.a.	n.a.	–	n.a.	n.a.	–	0.09	0.11	–	1.08
Pyrite 1a	×	–	46.26	0.49	52.56	0.05	–	0.02	–	–	n.a.	n.a.	n.a.	99.40
n = 98	SD	–	0.85	0.49	0.69	0.03	–	0.05	–	–	n.a.	n.a.	n.a.	0.86
Pyrite 1b	×	–	46.47	0.39	52.83	0.04	–	0.03	–	–	n.a.	n.a.	n.a.	99.78
n = 12	SD	–	0.94	0.40	0.39	0.01	–	0.04	–	–	n.a.	n.a.	n.a.	0.86
Arsenopyrite	×	–	33.86	43.80	20.91	0.09	n.a.	0.05	n.a.	–	n.a.	n.a.	n.a.	98.72
n = 49	SD	–	0.54	2.90	0.70	0.17	n.a.	0.11	n.a.	–	n.a.	n.a.	n.a.	2.53
D.L.		0.19	0.01	0.24	0.02	0.03	0.03	0.02	0.02	0.05	0.13	0.29	0.10	
INAA data [ppm]														
Sulphide separates		39.6	39.4	4800	n.a.	120	n.a.	400	99	33	–	7	n.a.	
Suphide separates		126	47.1	2700	n.a.	150	n.a.	230	–	24	9	4	n.a.	
D.L.		5 (ppb)	100	2	n.a.	5	n.a.	50	50	0.2	5	1	n.a.	

values of 32.2 to 32.8 atomic % are common. Values for nickel, cobalt, and antimony are generally < 0.1 wt.%.

Mineralizing fluids

Chlorite geothermometry

The chemical composition of chlorite is closely related to the formation temperature and may be calculated with the six-component chlorite solid solution model after Walshe (1986) or chlorite geothermometers after Krandiotis and MacLean (1987), Chatelineau (1988), and Jowett (1991). All geothermometers mainly base on the temperature dependence of aluminium within the tetraeder position of the chlorite lattice, assuming that chlorites coexist with quartz and an aqueous phase. Walshe (1986) additionally considered the redox state of iron and the H_2O content of the chlorites, which results in differences of the calculated structural formula and the given temperature of formation ($\sim$40 °C lower compared to other chlorite geothermometers). The advantages of the six-component chlorite solid solution model after Walshe (1986) refer to selective temperature calculation at either atmospheric pressure or at 1 kbar and to definition of further physico-chemical parameters of chlorite formation, e.g., fO_2, and in the presence of an iron sulphide additionally fS_2, and aH_2S.

Chlorite from the Ford mine, which formed during biotite alteration as well as during alteration of mafic minerals in xenoliths, is likely to have been formed cogenetic with pyrite (see Fig. 9G). Although hydrothermal quartz is not present, it is assumed that the system was sufficiently SiO_2-buffered. SiO_2 has been remobilized during chloritization of biotite and serizitization of K-feldspar and plagioclase (reactions 1, 4, and 5, Table 1), but probably was completely consumed during secondary K-feldspar formation and albitization of plagioclase (reactions 6 and 7, Table 1).

Chlorite was analyzed by electron microprobe (ARL-SEMQ) and classified according to Hey (1954) (Fig. 12).

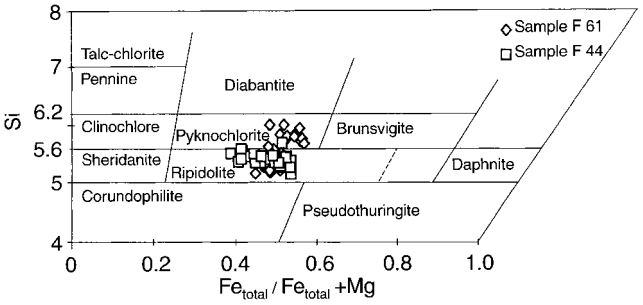

Fig. 12 Classification diagram for chlorites after Hey (1954) with position of chlorites from the mineralized granite (sample F 61, pyknochlorite and ripidolite compositions) and mineralized mafic xenolithes (sample F44, mainly ripidolite composition)

Table 4 Chemical analyses of chlorites (EPMA data) from altered granite and altered mafic xenoliths as well as calculated structural formula of chlorites and physico-chemical parameters using the CHLORITE computer programme after Walshe (1986)

	Chlorites in altered granite sample F 61 $n = 57$				Chlorites in altered mafic xenolithes sample F 44 $n = 30$			
Wt.%	Minimum	Maximum	Average	SD	Minimum	Maximum	Average	SD
Chemical composition (wt.%)								
SiO_2	29.68	25.87	26.55	0.82	27.05	24.67	25.85	0.62
TiO_2	0.25	0.09	0.49	1.06	0.07	0.08	0.09	0.09
Al_2O_3	20.78	22.47	20.39	1.52	21.23	21.48	20.95	0.52
FeO	23.14	24.71	26.62	1.05	21.15	27.99	25.59	2.04
MnO	0.07	0.14	0.10	0.03	–	0.16	0.12	0.03
MgO	13.85	16.94	15.03	0.83	16.62	13.53	14.71	1.32
CaO	–	–	0.03	0.07	0.07	–	0.09	0.09
Total	87.77	90.22	89.21		86.19	87.91	87.4	
Structural formula of chlorite on the basis of $O_{10}(OH)_8$								
Si	3.01	2.59	2.75	0.11	2.79	2.59	2.72	0.05
Al	0.82	1.20	1.05	0.10	1.06	1.17	1.09	0.03
Fe^{3+}	0.17	0.21	0.20	0.02	0.15	0.24	0.19	0.02
tet.	4.00	4.00	4.00		4.00	4.00	4.00	
Al	1.67	1.46	1.41	0.07	1.53	1.49	1.46	0.05
Fe^{3+}	0.23	0.21	0.25	0.02	0.20	0.25	0.23	0.02
Fe^{2+}	1.57	1.65	1.87	0.13	1.47	1.97	1.76	0.18
Mg + Mn	2.10	2.54	2.30	0.11	2.56	2.13	2.36	0.23
Oct.	5.57	5.86	5.83		5.76	5.84	5.81	
Physico-chemical parameters								
T(°C)	169	349	268	45	250	329	279	20
Log $f(O_2)$	−48.6	−26	−35.9	5.9	−36.5	−29.1	−33.9	2.3
Log $f(S_2)$	−19	−7.2	−12.2	3.1	−12.7	−8.9	−11.2	1.2
Log $a(H_2S)$	−3.6	−2.4	−2.7	0.3	3	−2.3	−2.7	0.2

Analyses of 56 chlorites from less carbonate altered, chloritized dark mica locally abundant in the K-feldspar-albite-sericite-pyrite zone gave a pycnochlorite and ripidolite composition (sample F 61; location close to F42, Table 2). Analyses of 20 chlorites in a mineralized mafic xenolith from the same zone gave a ripidolite composition (sample F44; close to F42, Table 2). The physico-chemical parameters have been calculated with the computer program CHLORITE (modified PC version after Walshe 1986) (Table 4). The data range is narrow for chlorites in the mafic xenolith and wider for chlorites in the altered granite. Average formation temperatures are ~270 °C (sample F 61) and ~280 °C (sample F 44), log $f(O_2)$ is ~−35 bar, log $f(S_2)$ ~−12 bar, and log aH_2S is −2.7 mol, assuming a confining pressure of 1 kbar (Fig. 13A–C). The reducing nature of the fluid is indicated by the majority of data points plotting within the magnetite-pyrite stability field. Chlorite formation between 240 °C and 340 °C occurred under elevated fS_2 and supports the argument that chlorite and pyrite (± gold) are cogenetic.

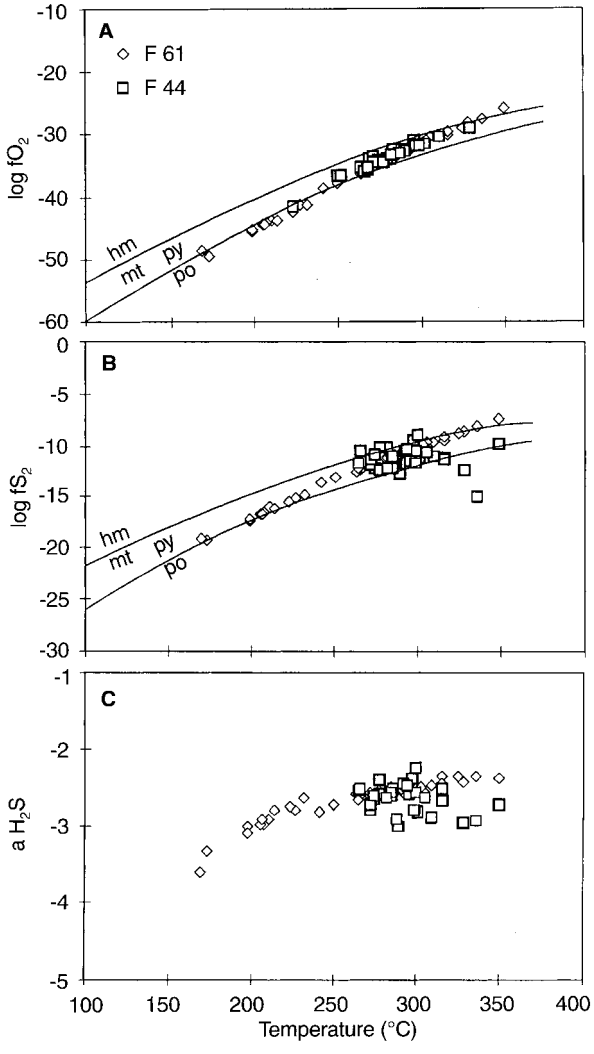

Fig. 13 **A** Temperature/log fO_2, **B** log fS_2, and **C** log a H_2S diagrams of chlorites from mineralized granite (sample F 61) and mafic xenolithes (sample F 44) of the Ford mine. Physico-chemical conditions were calculated based on microanalytical data (see Table 4) and application of the chlorite geothermometer after Walshe (1986) at 1 kbar (*hm-mt*, hematite-magnetite buffer line; *py-po*, pyrite-pyrrhotite buffer line)

Microthermometry

Fluid inclusions have only been found within trails in magmatic quartz phenocrysts. Fluids trapped in these trails are late- to postmagmatic and their suggested formation may be either syn- or postalteration and mineralization. The number of fluid inclusions in quartz suitable for microthermometric measurements (> 5 μm) is extremely limited in the investigated samples (12 thin sections). Therefore, the number of measurements presented here is low (~40 fluid inclusions). However, fluid inclusion studies were mainly carried out to find out, whether high salinity fluid inclusions (with daughter crystals) may occur, as those are indicative for a possible porphyry-related ore deposition. The investigated samples were taken from the K-feldspar-albite-sericite-pyrite zone, which could be correlated to the potassic zone found in many porphyry copper deposits bearing the highest temperature and salinity of fluid inclusions (Roedder 1984).

Two types of fluid inclusions are noted: (1) Three-phase inclusions of type I [$H_2O(l) + CO_2(l) + CO_2(v)$] occur in isolation and along trails within the magmatic quartz. They range between < 5–15 μm in size and have a degree of filling of 60–90 vol.% CO_2 (L + V). (2) Two-phase inclusions of type II [$H_2O(l + v)$] have negative crystal shapes and are found in trails. They have a size of < 5–10 μm and a degree of filling of 75–85 vol.% L. Daughter crystals were not observed. Inclusions of types I and II do not occur on the same trail, crosscutting relationships of the trails were not observed.

Heating consistently lead to homogenization into the liquid phase. Type I and II inclusions give heating-freezing results as follows:

1) Type I: Th_{CO_2} = 27–30 °C, $Th_{CO_2-H_2O}$ = 270–310 °C, Tm_{CO_2} = −58.1 °C to −56.6, $Tm_{clathrat}$ = 3.4–7.3 °C (Fig. 14);
2) Type II: Th = 190–260 °C (Fig. 14), Tm = −5.4 to −0.9 °C, Te = ≥ −7.8 °C (only 10 measurements for Tm/Te possible, data not shown).

Assuming a lithostatic pressure ≤1 kbar (see discussion), formation temperatures range between 250 °C and 335 °C (for 5 wt.% NaCl equivalent; pressure correction after Zhang and Frantz 1987).

Isotope data

Analytical techniques

Stable isotope analyses were carried out on sulphides and carbonate from the K-feldspar-albite-sericite-pyrite zone (location of

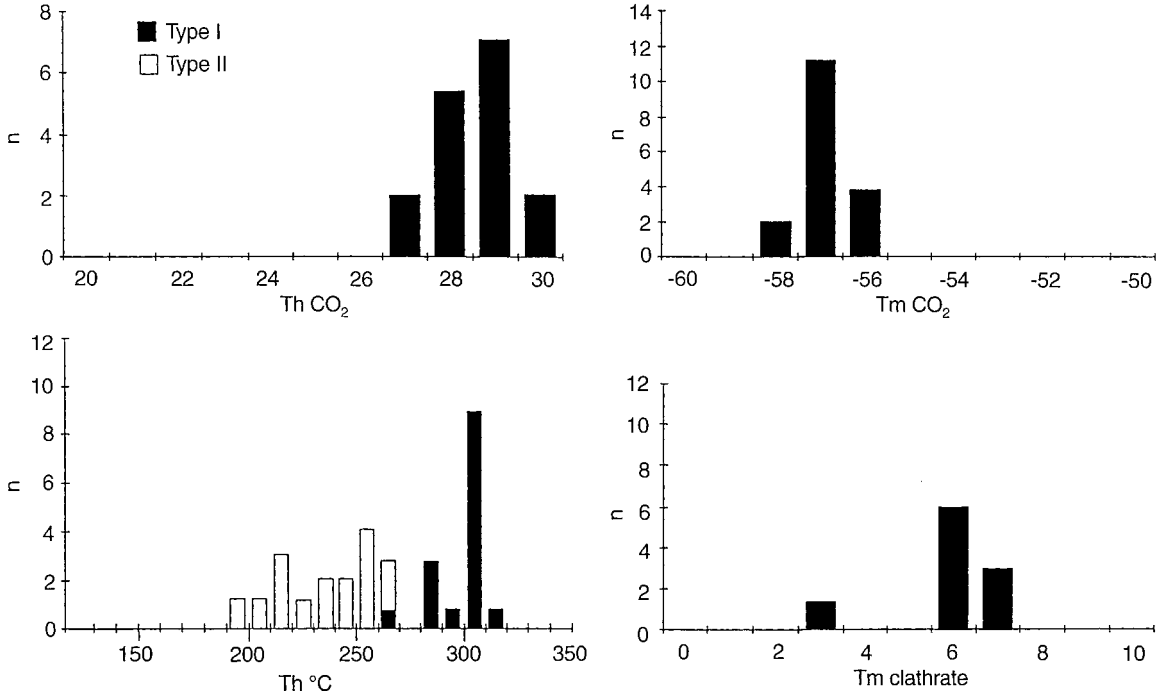

Fig. 14 Microthermometric data of secondary fluid inclusions of *types I* (three phase CO_2-H_2O) and *II* (two phase H_2O) in porphyritic magmatic quartz of the mineralized K-feldspar-albite-sericite-pyrite zone

samples P2 and P3 is close to sample P1, Fig. 3; Table 5). The analytical procedures are described in Ueda and Krouse (1986) and McCrea (1950). Measurements were made on a Finnigan Delta mass spectrometer. Whole-rock sulphur was extracted by Kiba reagent (Kiba et al. 1955).

Zircon, monazite, ilmenite and pyrite of the K-feldspar-albite-sericite-pyrite zone have been analyzed for U/Pb and Pb/Pb (sample P1, Fig. 3; Tables 6 and 7). Three fractions of zircon were dissolved in modified Krogh-style teflon bombs in 48% HF for 6 days at 190 °C. Pb and U were separated on DOWEX AG 1 × 8-charged miniaturized 100 µlt Teflon colums, using both HBr-HCl and HNO_3 elution recipes. The total procedural blank was ~45 pg Pb. Pb was loaded together with silica gel and phosphoric acid and measured from 20 mm Re filaments on a VG Sector mass-spectrometer in static mode. Fractionation amounted to 0.085 ± 13%/AMU ($n = 85$), determined on repeat analyses of the NBS 981 Pb standard. U was analyzed using a Ta-Re-Ta triple filament configuration on a single cup AVCO mass-spectrometer (Table 6). Stepwise Pb leaching (PbSL) (modified after Frei and Kamber 1995) was performed on a 100–140 µm fraction of pyrite and on a mixed concentrate of subordinate pyrite, ilmenite, zircon and monazite. The types of acids and the duration of leaching for the individual steps are indicated in Table 7. Pb from the leachates and the residues was separated on 0.5 ml DOWEX AG 1 × 8-charged quartz glass columns using a standardized HBr-HCl recipe. This procedure added a non-decisive blank of < 300 pg. Errors (reported at the 2σ level) and correlation coefficients (*r*'s) were calculated after Ludwig (1980, 1990).

Table 5 Stable isotope data of calcite and sulphides (pyrite and minor arsenopyrite) from the Ford gold deposit (all samples are located close to sample P1, see Fig. 3)

Sample	Location	$\delta^{18}O$ [‰] SMOW	$\delta^{13}C$ [‰] PDB	$\delta^{34}S$ [‰] CDT
P1	Whole-rock calcite	12.7	−6.2	
P2	Whole-rock calcite	12.2	−6.4	
P3	Whole-rock calcite	11.9	−6.4	
P1	Py/apy separate			2.7
P2	Py/apy separate			1.8
P3	Py/apy separate			−1.4
P4	Whole-rock sulfur			2.6

S, O, and C stable isotope data

Three pyrite-arsenopyrite separates from the K-feldspar-albite-sericite-pyrite zone give $\delta^{34}S$ values of −1.4‰ to 2.7‰ (Fig. 15, Table 5), defining a relatively narrow 4.1‰ range. Whole-rock sulphur of one sample of the same alteration zone has a $\delta^{34}S$ value of 2.6‰. The $\delta^{18}O$ values of whole-rock calcite are between 11.9‰ and 12.7‰, the $\delta^{13}C$ values are between −6.2‰ and −6.4‰

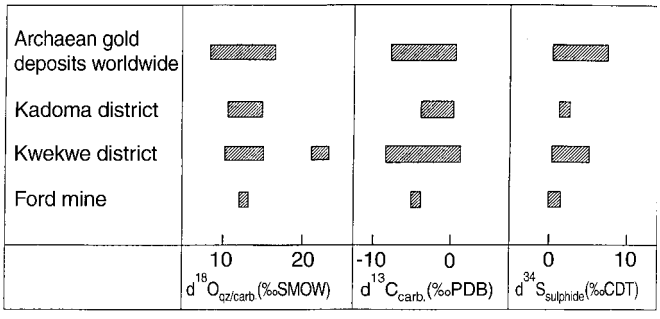

Fig. 15 Stable isotope data of sulphides and calcite from the Ford mine compared to stable isotope data from shear zone hosted gold deposits in the Kwekwe (Buchholz 1995) and Kadoma (Herrington 1991; Carter 1990) districts and Archaean gold deposits world wide (Groves and Foster 1991)

(Table 5). Small variations in the isotopic data are most probably related to small-scale changes of the physico-chemical conditions during mineralization (see Ohmoto 1986). The stable isotope data is similar to results obtained for several shear-zone hosted gold and gold-antimony deposits in the Kwekwe (Buchholz 1995) and Kadoma (Carter 1990; Herrington 1991) districts, and for many Archaean gold deposits world wide (Groves and Foster 1991) (Fig. 15).

U/Pb and Pb/Pb isotope data

Separated zircons were brownish-cloudy and commonly had inclusions of a black opaque mineral. They were strongly corroded, resulting in rounded shapes. The zircon fractions are characterized by low $^{206}Pb/^{204}Pb$, probably resulting from both initially high common Pb contents and Pb-rich opaque inclusions (Table 6). U-Pb and Pb-Pb ages were calculated assuming precise knowledge of the initially built-in common Pb composition. The initially built-in common Pb was taken from the least radiogenic PbSL analysis (h[4], see Table 7) of a heavy mineral concentrate composed of zircon, monazite, illmenite and minor amounts of pyrite. Age data are highly discordant, with $^{207}Pb/^{206}Pb$ ages of ~2550 Ma, suggesting Pb-loss to have happened at some relatively recent time.

Variably radiogenic Pb was recovered from the individual acid leach steps of the heavy mineral concentrate (Table 7). Strong nitric acid released a highly thorogenic Pb component which is attributed to the influence and response of monazite, whereas the first 4N HNO_3 step dissolved a common Pb-bearing phase, most probably ilmenite. This unradiogenic Pb was taken as the correction Pb for the U-Pb zircon analyses. The last three step leachates (H[4]–H[6]; primary igneous minerals) and the three zircon bulk analyses define an isochron of 2541 ± 17 Ma (MSWD = 0.65) (Fig. 16A), which is interpreted as the intrusion age of the granite dike.

Data from the first three step leachates lie off this reference line, possibly indicating variable degrees of contamination by minor amounts of pyrite (easily affected by bromic acid) in the heavy mineral separate. This interpretation is consistent with step leach data of the pyrite fraction (Fig. 16B) which are characterized by slightly elevated $^{207}Pb/^{204}Pb$ values relative to the reference isochron. The first four step leach data of pyrite yield a linear array in the uranogenic diagram of Fig. 16B, with meaningless geological age constraint. The line is interpreted as a mixing line, involving both a Pb component from the granite and one with elevated μ-characteristics. Pb with elevated μ-characteristics most probably has to be sought in an evolved continental crust, as exemplified, for example, by ~2700 Ma Shamvaian metasediments (Pb isotope data are from Jelsma 1993) which commonly discordantly overlie upper greenstone successions in Zimbabwe and are also present in the Midlands greenstones.

Table 6 Conventional U-Pb isotope data of zircon from the Ford granite

Sample	Fraction (μm)	Weight (mg)	$^{206}Pb/^{204}Pb$ (meas.)	U (ppm)	Pb_{rad} (ppm)	Pb_{tot} (ppm)	$^{207}Pb/^{206}Pb$	±2σ (%)	$^{207}Pb/^{235}U$	±2σ (%)	$^{207}Pb/^{236}U$ (Ma)	±2σ	$^{206}Pb/^{236}U$ (Ma)	±2σ	$^{207}Pb/^{206}Pb$ (Ma)	+2σ	−2σ	r
P1	40–60	0.68	58	130	38	83	0.16816	1.26	5.41430	1.57	0.23352	0.67	1887.1	29.6	1352.9	9.1	2539.4	21.0	21.4	0.624
	60–80	1.52	48	75	23	57	0.17086	1.69	5.26574	1.98	0.22352	0.57	1863.3	36.9	1300.4	7.5	2566.1	27.9	28.5	0.622
	80–100	0.91	46	113	39	98	0.17468	1.78	5.86787	2.09	0.24363	0.53	1956.5	40.8	1405.6	7.5	2603.0	29.4	30.0	0.658

Data corrected for common Pb using composition of step leachate h[4] in Table 2
Procedural Pb blank < 45 pg
Correlation coefficient *r* calculated after Ludwig (1980)

Table 7 Stepwise Pb-leaching and bulk Pb isotope data from the Ford granite

Sample, mineral[a], size fraction[b]	Technique	Step [nr]	Acid (PbSL)	Time	$^{206}Pb/^{204}Pb$	$\pm 2\sigma^{a}$	$^{207}Pb/^{204}Pb$	$\pm 2\sigma^{a}$	$^{208}Pb/^{204}Pb$	$\pm 2\sigma^{a}$	r_1^{c}	r_2^{d}
P1 Py 100–140	PbSL	p[1]	4N HBr	10′	31.160	0.021	18.368	0.014	44.186	0.037	0.965	0.924
Py 100–140	PbSL	p[2]	4N HBr	40′	30.328	0.035	18.259	0.022	43.727	0.059	0.969	0.902
Py 100–140	PbSL	p[3]	4N HBr	3 h	29.808	0.117	18.240	0.072	43.531	0.175	0.990	0.979
Py 100–140	PbSL	p[4]	8N HBr	12 h	29.238	0.049	18.170	0.032	43.560	0.084	0.956	0.879
Py 100–140	PbSL	p[5]	8N HBr	18 h	28.259	0.195	17.935	0.125	43.771	0.304	0.992	0.996
Heavy mineral concentrate	PbSL	h[1]	4N HBr	10′	30.534	0.142	18.211	0.086	43.933	0.206	0.993	0.995
Heavy mineral concentrate	PbSL	h[2]	4N HBr	3 h	31.223	0.239	18.218	0.140	47.558	0.365	0.996	0.998
Heavy mineral concentrate	PbSL	h[3]	4N HBr	12 h	33.150	0.068	18.533	0.039	67.439	0.143	0.989	0.988
Heavy mineral concentrate	PbSL	h[4]	4N HNO_3	6 h	17.607	0.088	15.719	0.080	36.130	0.183	0.994	0.996
Heavy mineral concentrate	PbSL	h[5]	14N HNO_3	10 h	44.189	0.316	20.231	0.145	122.845	0.882	0.997	0.999
Heavy mineral concentrate	PbSL	h[6]	48% HF + 14N HNO_3	2 d	90.853	0.784	28.033	0.242	55.748	0.482	0.998	0.999
Zrn 40–60	bulk	z[1]			58.253	0.879	22.569	0.342	47.476	0.719	0.997	0.996
Zrn 60–80	bulk	z[2]			47.752	0.826	20.887	0.362	48.531	0.841	0.998	0.999
Zrn 80–100	bulk	z[3]			46.123	1.039	20.704	0.467	50.052	1.129	0.998	0.999

[a] Py, pyrite; Zrn, zircon; heavy mineral concentrate, ± pyrite, ilmenite, monazite, zircon
[b] Grain size fraction in µm
[c] r_1, $^{206}Pb/^{204}Pb$ versus $^{207}Pb/^{204}Pb$ error correlation (Ludwig 1980)
[d] r_2, $^{206}Pb/^{204}Pb$ versus $^{208}Pb/^{204}Pb$ error correction (Ludwig 1980)
[e] Errors are two standard deviations absolute (Ludwig 1980)

Fig. 16 **A** Pb/Pb diagram with bulk data from zircon (*z*) and stepwise Pb-leaching (PbSL) data (*h*) of the Ford porphyrtic granite. *Numbers in square brackets* correspond to grain size fractions for zircons (see Table 6) and to step leachates for PbSL analyses (see Table 7). An isochron age of 2541 ± 17 Ma through the zircon data and the last three step analyses of the heavy minerals is interpreted as the intrusion age of the Ford porphyritic granite. *Boxed area is enlarged* in **B**. **B** Enlarged area with stepwise Pb-leaching (PbSL) data of the heavy minerals (*h*) and a gold-bearing pyrite (*p*) fraction from the Ford deposit. *Numbers in square brackets* correspond to steps of the PbSL analyses (Table 7). PbSL data from pyrite, except the residual analysis (*[5]*), define a linear trend which is interpreted to represent a mixing line between a Pb component from the porphyry and one derived from metasediments pertaining to the greenstone succession. The first three PbSL analyses ([h 1, 2, 3]) of the heavy minerals do not fall on the isochron of 2541 ± 17 Ma, but instead are contaminated by Pb from pyrite. *Area filled with crosses* comprises Pb isotope data from other porphyritic intrusions in the Harare-Shamva greenstone belt and data from Shamvaian metasediments (Jelsma 1993)

Discussion of porphyry-related versus shear-zone related gold mineralization

Arguments for porphyry-related gold mineralization

Archaean porphyry gold deposits have been discussed extensively in the past, but no clear evidence for an orthomagmatic-hydrothermal genesis has been reported. Based on a study on gold-bearing porphyry copper systems, Sillitoe (1979, 1991) predicted the existence of such deposits in Phanerozoic volcano-plutonic arcs and possibly in Archaean greenstone belts. Phanerozoic,

copper deficient, porphyry gold deposits have already been recognized (e.g., Marte deposit in Chile; Vila et al. 1991).

Porphyry deposits are generally characterized by a sub-volcanic intrusion level (3–5 km depth) of large (several kilometers across) granitoid plutons, a typical disseminated and stockwork-type mineralization, and significant alteration zonation within the pluton and the host rocks. The close spatial relationship of mineralization with porphyritic intrusions indicate the involvement of magmatic fluids. Fluid inclusion studies show that early mineralization stages within the central potassic zone (K-feldspar-biotite-Cu-sulphides-magnetite) are dominated by 700–800 °C, high salinity (up to >60 wt.% NaCl equivalent) fluids coexisting with gas-rich (CO_2-bearing), low salinity (1–2 wt.% NaCl equivalent) fluids. Late stage mineralization is characterized by involvement of meteoric fluids, pyrite formation, and sericite, chlorite, as well as argillitic alteration at relatively low temperatures (200–300 °C). Stable isotope data of ore and gangue minerals are relatively variable ($\delta^{18}O = 6–9‰$; $\delta D = -35$ to $-75‰$; $\delta^{34}S = -3$ to $+9‰$) and indicate mixing trends between magmatic and meteoric fluids (see e.g., Sillitoe 1991 and references therein; Hedenquist 1996).

Four major field observations characteristic of porphyry deposits are noted at the Ford gold mine:

1. Gold and sulphide mineralization is closely associated with metasomatism and development of an inner K-Feldspar-albite-sericite-pyrite (±biotite?, potassic zone?) and an outer propylitic alteration zone within porphyritic granite, which is spatially confined to the s-shaped portion of the granite dike intrusion. The K-Feldspar-albite-sericite-pyrite zone is characterized by a greenish color, secondary K-feldspar formation spatially and probably genetically related to pyrite precipitation, replacement of magmatic plagioclase by albite, absence of secondary quartz as well as less altered dark mica (formerly primary biotite or secondary mica?). However, secondary feldspars (K-feldspar-albite) occur in many Archaean granite-hosted and shear-zone related gold deposits as well (Keays and Skinner 1989; Cassidy and Bennet 1993), but alteration pattern found at Ford is extremely uncommon;
2. Major shear zones and gold-quartz veins, commonly hosting the gold in the Kwekwe district, are absent within the orebody, at least not recognizable at the current stage of open pit mining;
3. Gold and sulphides occur as disseminations throughout the orebody;
4. Veinlets observed in one drillcore sample might indicate stockwork mineralization at depth. Several porphyritic dikes of granitoid composition occur in the area and are partly mineralized; they may belong to a specific intrusive suite favorable for gold transport and deposition. Regional petrologic investigations on porphyritic dikes in the area between the Indarama and Jojo mines have been initiated (R.Wormald, personal communication 1995, 1997).

Arguments for shear-zone related gold mineralization

Nutt et al. (1988a) and Darbyshire et al. (1996) showed that shear-zone related gold mineralization in the Midlands greenstone belt, like other greenstone belts of Zimbabwe (e.g., Vinyu et al. in press), is mainly of late Archaean to early Proterozoic age. A first stage of gold mineralization in the Midlands greenstone belt has been correlated with the emplacement of trondhjemite-tonalite-granodiorite intrusions, e.g., the Sesombi tonalite NW of Kwekwe (2.570 ± 42 Ma; Darbyshire et al. 1996; Stowe 1979). The second stage of gold mineralization at 2.410 ± 70 Ma (Darbyshire et al. 1996) has been interpreted to be genetically related to the intrusion of the Great Dike and subsequent reactivation of "master shears", e.g., the TMDZ and SDZ.

Arguments for shear-zone related gold mineralization at the Ford mine mainly base on the regional structural setting and deformation textures in primary magmatic quartz, Pb isotopic data of primary magmatic minerals versus pyrite, ore mineralogy and geochemistry, and subordinately on fluid inclusion and stable isotope studies.

1. The regional structural setting of the Ford deposit indicates that intrusion of the granite occurred into the metavolcanic sequence along a tension gash during sinistral movement of the Taba-Mali- and Sherwood deformation zones (Fig. 2 and Fig. 17A,B). Opposite reactivation of the deformation zones is indicated by twisting of the WNW- and SSE endings of the granite dike and aggrees with the findings of major dextral reactivation in the Kwekwe district (Campbell and Pitfield 1994) (Fig. 17C). The fact that gold mineralization only occurs within the s-shaped part of the dike may point to a direct relationship between regional deformation and alteration and gold mineralization of the granite (Fig. 17D). The main question, whether s-type deformation of the dike and mineralization still occurred during hot, ductile conditions, remains open. Several examples from Australian gold deposits have shown that melts and gold-bearing fluids may use the same dilational structures for ascent during clearly separated events (Perring et al. 1991). Syntectonic emplacement of gold-arsenic-bearing fluids within a stillhot granite body may be envisaged as a possible scenario for the genesis of the Ford deposit. The absence of major veins and shear zones, as well as the homogeneous distribution of pyrite and gold in the orebody, may point to a rather semiplastic character of the granite over a relatively wide area. Deformation bands of quartz phenocrysts show that strong deformation occurred at least in some parts of the orebody. However, detailed structural investigations were not possible at the stage of exploration and mining in 1992/1993.

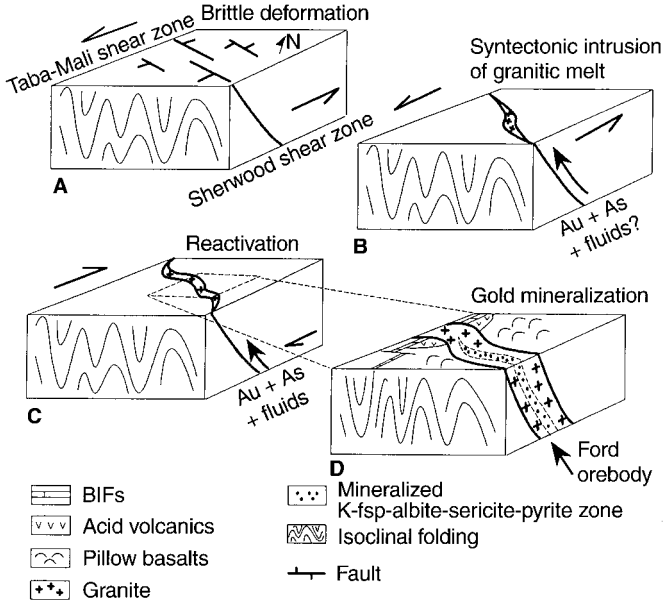

Fig. 17A–D Simplified genetic concept for gold mineralization at the Ford mine. **A** Sinistral displacement along the Taba-Mali and Sherwood shear zones and brittle deformation within the volcano-sedimentary sequence of the Upper Bulawayan; **B** granite intrusion along second order fractures and syntectonic deformation; **C** re-activation of the Taba-Mali and Sherwood shear zones with dextral displacement caused twisting of the WNW-SSE endings of the granite dike. Gold mineralization only occurs in the s-shaped part of the intrusion. Gold- and arsenic-bearing fluids were precipitated either during the late cooling stage within an area of high deformation (**B**) or during later reactivation of the shear zones (**C**). **D** The orebody is characterized by alteration zoning with a central K-feldspar-albite-sericite pyrite zone and a marginal propylitic zone (**D**, detailed sketch of **C**)

2. Pb isotopic studies show that pyrite (and possibly gold) is not in isotopic equilibrium with accessory magmatic phases of the host granite at Ford mine, therefore implying an additional, non-magmatic source of Pb. The Pb isotope composition of pyrite additionally differs from that of typical Archaean shear-zone hosted gold mineralization, in that a clear contamination of the fluid is indicated. Because of the small size of the intrusion in comparison to porphyry deposits it is suggested that Pb isotopic contamination did not result through mixing of magmatic with heated meteoric fluids circulating within the nearby country rocks. Host rocks along both sides of the unmineralized granite dike WNW and SSE of the orebody, as well as of similar dikes in the nearby Indarama mine area, are only weakly altered. Low alteration in these locations shows that the granite dike intrusion was generally fluid-poor. Country rocks at the immediate contact to the mineralized granite dike in the NE and SW (profiles 1 and 2, Fig. 10) are characterized by a narrow Na-K-As alteration, instead. Alteration of the country rocks at these locations rather seems to be related to later, post-magmatic fluid circulation in the granite body.

Fluids could have been generated initially after a certain degree of crystallization of the granite melt, but if so, Pb isotopic composition of the primary magmatic minerals and pyrite should be similar. Stepwise Pb leaching data from gold-bearing pyrite of the Ford granite reveal contamination of the mineralizing fluid at depth by an evolved older continental crust and suggest a late to postmagmatic ($< 2541 \pm 17$ Ma) deep crustal fluid (contaminated metamorphic fluid?) percolating through the Ford orebody. In addition, the Pb isotope characteristics of the magmatic phases of the porphyritic granite at Ford mine are compatible with the signatures of other late Archaean porphyritic intrusions emplaced in Zimbabwean greenstone belts (data from Jelsma 1993) and suggest a late Archaean magmatism with very homogeneous Pb sources over a wide area. For some deposits, for example for the Mazowe mine (Harare-Shamva greenstone belt), it has been shown that Pb from spatially associated granitoids was more or less in equilibrium with Pb from the mineralization and the associated cogenetic alteration minerals. Pb isotopic equilibrium of these minerals suggests a close genetic relationship between late Archaean intrusions and shear-zone hosted Au mineralization at least in some areas (Vinyu et al. in press). On the other hand, recent findings by Frei and Pettke (1996) describe late Proterozoic Au mineralization along reactivated Archaean shear zones in the Harare-Shamva greenstone belt and correlate this mineralization with major Proterozoic tectono-metamorphic events at the craton's borders and with intracratonic rifting.

3. Ore geochemistry and ore mineral paragenesis at the Ford mine are rather simple. Au and As are enriched, other ore metals commonly elevated in porphyry deposits such as Cu, Mo, Zn, Te, Bi, Hg are lacking or are not systematically elevated. Although copper and other ore metals are generally not widespread in Archaean gold deposits worldwide, they are elevated in an Archaean Cu-porphyry-style mineralization e.g., at the Miralga Creek prospect in the Pilbara block (Australia, Goellnicht et al. 1988). Ore mineralogy comprises native gold, pyrite and minor amounts of arsenopyrite and electrum. In contrast, Phanerozoic gold porphyries are characterized by a dominance of pyrite, magnetite and gold, but small amounts of chalcopyrite, enargite, bornite, tennantite or molybdenite are usually present (e.g., Vila et al. 1991). Even at the Miralga Creek prospect, pyrite, chalcopyrite, sphalerite, galena, tetrahedrite and Ag-minerals have been described (Goellnicht et al. 1988). Typical stockworks, besides one unclear drill core sample with crosscutting veinlets (Fig. 5, sample 3), or at least hydrothermal breccias have not yet been discovered at the Ford mine, although they may occur at further depth.

Several arguments point to a shear-zone related rather than a porphyry-related gold mineralization. They include temperature data, composition of fluid inclusions,

and stable isotope data in comparison with data of shear-zone hosted gold deposits in the Kwekwe district.

Gold mineralization is assumed to have taken place during metasomatic processes under elevated Na^+ and K^+ activity (formation of postmagmatic K-feldspar and albite), high sulphur fugacity (pyrite/arsenopyrite deposition), and moderate temperatures and pressures. Conditions of deposition are estimated at a minimum of 220–330 °C (chlorite formation, pressure-corrected fluid inclusion data), a maximum of 1.5 kbar (subvolcanic level), and on a H_2S activity $\geq 10^{-3}$ mol (34 ppm). Carbonate alteration of biotite and plagioclase must have taken place under elevated CO_2 concentrations supported by fluid inclusion studies of quartz phenocrysts. The CO_2-bearing fluids were of low salinity (maximum 8 wt.% NaCl equivalent), which is characteristic of many Archaean gold deposits of the Midlands and other greenstone belts worldwide (e.g., Groves and Phillips 1987; Kerrich 1989; Phillips and Powell 1993; Buchholz 1995). High gold values (up to 7 ppm) conspicuous in the transition between the K-feldspar-albite-sericite-pyrite and the propylitic zones may imply rapid decrease in temperature or sulphur fugacity of the fluid, which caused instability of gold complexes (see Seward 1991; Hayashi and Ohmoto 1991) and subsequent gold deposition within that zone. However, the salinity and temperature data described are common for low temperature alteration zones in porphyry deposits as well. The missing high temperature and high salinity zone may not have been exposed yet.

Carbon and oxygen stable isotope data of carbonates and sulphur stable isotope data of pyrite agree with that of gangue and ore minerals from late Archaean vein-type and shear zone hosted gold mineralization in the Kwekwe (Buchholz 1995; Porter and Foster 1991) and Kadoma (Herrington 1991; Carter 1990) districts, for which deep crustal probably metamorphic fluid sources have been discussed (Fig. 15). The similarity of the stable isotope data may point to a similar fluid source for the Ford deposits. Pb isotope data additionally indicate fluid interaction with sedimentary country rocks possibly of Shamvaian age at depth.

Summary and conclusions

Gold mineralization at the Ford mine is uncommon and has not been described in the Archaean of Zimbabwe before. Arguments for a porphyry- versus a shear-zone related type of gold mineralization have been discussed in this study. Features at the Ford mine supporting a porphyry-related gold mineralization are (1) alteration style with development of an inner K-feldspar-albite-sericite-pyrite and an outer propylitic zone in porphyritic granite; (2) absence of major shear zones and gold-quartz veins at the current stage of open pit mining; (3) disseminated pyrite mineralization throughout the orebody; and (4) veinlets observed in one drillcore sample that might indicate stockwork mineralization at further depth. All these arguments, however, do not exclude a shear-zone related type of gold mineralization. Arguments that support instead a shear-zone related type of gold mineralization include (1) regional structural constraints; (2) Pb isotope compositions of primary magmatic minerals versus ore minerals such as pyrite, and (3) ore geochemistry, ore mineralogy and ore textures.

The following concept is suggested: gold mineralization at the Ford mine occurred late to postmagmatic relative to the intrusion of the host porphyritic granite at $\leq 2541 \pm 17$ Ma, or later in the early Proterozoic. Intrusion of the granitic magma between the TMDZ and SDZ was probably followed by ascent of gold-, arsenic-, H_2S, and CO_2-bearing, low salinity fluids of 220–330 °C common in the late Archaean of the Kwekwe district. Granite melt and gold-bearing fluids of different source may have used the same dilational structures for ascent and were channelled along a second-order shear zone. Maximum dilation in the s-shaped part of the dike allowed percolation of the gold-bearing fluids through a more or less consolidated granitic rock. Gold, pyrite, and arsenopyrite deposition contemporaneous with the alteration and formation of greenish sericite, secondary K-feldspar, albite, and carbonates occurred from this fluid which likely interacted with sediments of the greenstone succession prior to ascent into the Ford granite.

The granite-hosted and disseminated gold mineralization may represent a new low-grade type of gold deposit hitherto unrecognized in the Archaean craton of Zimbabwe. The rediscovery of this deposit is economically important, in that it could potentially direct gold exploration towards similar late Archaean porphyritic intrusions occurring not only in the Midlands province, but also in other greenstone belts of Zimbabwe. Exploration should focus on (1) porphyritic granite intrusions syntectonically emplaced between two major strike slip deformation zones within brittly deformed rocks; (2) close age relationships between intrusion and regional gold mineralization; (3) dilational sites within the intrusion; and (4) recognition of an uncommon alteration mineralogy including secondary feldspars, disseminated pyrite, and greenish sericite, which gives the rock its atypical greenish color.

Acknowledgements The authors are particulary grateful to F.-W. Wellmer, T. Oberthür, H.-O. Angermeier, U. Vetter, and A. Höhndorf (BGR, Hannover) for guidance and helpful discussions during this study. The research project "Gold in porphyritic granite of the Ford mine, Kwekwe district, Zimbabwe" was commissioned and funded by the German Federal Institute for Geosciences and Natural Resources (BGR, Hannover) as a contribution to the BGR project "Metallogenesis of Gold in Africa". The Ford deposit was rediscovered during field work in April 1992 by P.B. during his Ph.D. thesis on gold mineralization in the Kwekwe district at Aachen University of Technology. A second field campaign has been carried out in 1993 for detailed sampling and mapping of the Ford deposit. We would like to thank the Geological Survey of Zimbabwe and the Boulder Mining Company (PVT) Ltd for logistic support. Special thanks for continuous support and hospitality at the Indarama mine are due to R. Flowerday (Director), T. Lahee (Mine Manager), E. Cattelino

(Metallurgist), and G. MacDonald (Mine Operator). We thank N. Mertes for help with geochemical and S. Littmann and J. Götze for cathodoluminescence analyses. We also wish to thank Jean-François Couture and one Associate Editor of *Mineralium Deposita* for their helpful and constructive reviews which greatly improved the manuscript.

References

Arita K, Sato J (1987) Report on the cooperative mineral exploration of Kadoma area (Phase 1). Japan International Cooperation Agency, Metal Mining Agency of Japan 29, 223 p

Buchholz P, Spaeth G, Friedrich G (1991) Gold antimony mineralization in Zimbabwe (in German). Berichte zur Lagerstätten- und Rohstofforschung 4, part 1, Bundesanstalt für Geowissenschaften und Rohstoffe, Hannover: 134 p

Buchholz P, Herzig P, Friedrich G (1993) Discovery of a gold deposit in the Kwekwe district: "Gold porphyries" in Archaean greenstone belts in Zimbabwe? Sub-Saharan Economic Geol Conf Abstr, Harare: 1–2

Buchholz P, Friedrich G, Herzig P (1994) Gold-Antimony mineralization in the Zimbabwe Craton: the Indarama mine at Kwekwe and the Belingwe Star mine at Mberengwa. In: Oberthür T (ed) Metallogenesis of selected gold deposits in Africa. Geol Jahrb, Reihe D 100, Bundesanstalt für Geowissenschaften und Rohstoffe Hannover, pp 343–390

Buchholz P (1995) Gold mineralization in the Kwekwe district, Midlands greenstone belt, Zimbabwe (German). PhD Thesis, Institut für Mineralogie und Lagerstättenlehre, RWTH Aachen, Aachener Geowissenschaft Beitr 9, Aachen, 266 p

Burrows DR, Spooner ETC (1989) Relationship between Archean gold quartz vein-shear zone mineralization and igneous intrusions in the Val d'Or and Timmins areas, Abitibi Subprovince, Canada. In: Keays RR, Ramsay WRH, Groves DI (eds) The geology of gold deposits: the perspective in 1988. Econ Geol Monogr 6: 424–444

Cameron EM, Hattori K (1987) Archean gold mineralization and oxidized hydrothermal fluids. Econ Geol 82: 1177–1191

Campbell SDG, Pitfield PEJ (1994) Structural controls of gold mineralization in the Zimbabwe craton – exploration guidelines. Zimbabwe Geological Survey Bulletin 101, Harare, 270 p

Carter AHCh (1990) Fluid-rock interaction and gold deposition within a late Archaean shear zone, Dalny Mine, Zimbabwe. PhD Thesis, Department of Geology, The University of Southampton, UK, 332 p

Cassidy KF, Bennet JM (1993) Gold mineralisation at the Lady Bountiful Mine, Western Australia: an example of a granitoid-hosted Archaean lode gold deposit. Mineralium Deposita 6: 388–408

Cathelineau M (1988) Cation site occupancy in chlorites and illites as a function of temperature. Clay Miner 23: 471–485

Darbyshire DPF, Pitfield PEJ, Campbell SDG (1996) Late Archean and early Proterozoic gold-tungsten mineralization in the Zimbabwe Archean craton: Rb-Sr and Sm-Nd isotope constraints. Geology 24/1: 19–22

De la Roche H, Leterrier J, Grand Claude P, Marchal M (1980) A classification of volcanic and plutonic rocks using R1-R2 diagrams and major element analyses – its relationship with current nomenclature. Chem Geol 29: 183–210

Foster RP, Mann AG, Stowe CW, Wilson JF (1986) Archaean gold mineralization in Zimbabwe. In: Anhaeusser CR, Maske S (eds) Mineral deposits of Southern Africa. Geological Society South Africa 1, pp 43–112

Foster RP, Fabiani WMB, Carter AHC, Fisher NJ, Porter CW (1991) The tectonic magmatic framework of Archaean lode-gold mineralization in the Midlands greenstone belt, Zimbabwe. In: Ladeira EA (ed) Brazil Gold '91. AA Balkema, Rotterdam, pp 359–366

Fraser R (1993) The Lac Troilus gold-copper deposit, northwestern Quebec: a possible Archaean porphyry system. Econ Geol 88: 1685–1699

Frei R, Kamber BS (1995) Single minerals Pb-Pb-dating. Earth Planet Sci Lett 129: 261–268

Frei R, Pettke T (1996) Mono-sample Pb-Pb dating of pyrrhotite and tourmaline: Archean versus Proterozoic gold mineralization in Zimbabwe. Geology 24/9: 820–823

Friedrich G, Buchholz P, Herzig P (1996) Gold in porphyritic granite of the Ford mine, Kwekwe district, Zimbabwe (in German). Berichte zur Lagerstätten- und Rohstofforschung, Bundesanstalt für Geowissenschaften und Rohstoffe, Hannover, 27, 172 p

Goellnicht NM, Groves IM, Groves DI, Ho SE, McNaughton NJ (1988) A comparison between mesothermal gold deposits of the Yilgarn Block and gold mineralization at Telfer and Miralga Creek, Western Australia: indirect evidence for a non-magmatic origin for greenstone-hosted gold deposits. In: Ho SE, Groves DI (eds) Advances in understanding precambrian gold deposits, II, Geology Department and University Extension, The University of Western Australia, Perth, pp 309–320

Götze J (1994) Zur Kathodolumineszenz von SiO_2. European J Mineral 6: 78

Gresens RL (1967) Composition-volume relationships of metasomatism. Chem Geol 2: 47–65

Groves DI, Foster RP (1991) Archaean lode gold deposits. In: Foster RP (ed) Gold metallogeny and exploration. Blackie and Son, London, pp 63–103

Groves DI, Phillips GN (1987) The genesis and tectonic control on Archaean gold deposits of the western Australian shield – a metamorphic replacement model. Ore Geol Rev 2: 287–322

Harrison NM (1970) The geology of the country around Queque. Rhod Geol Surv Bull 67: 125

Hattori K (1987) Magnetic felsic intrusions associated with Canadian Archean gold deposits. Geology 15: 107–1111

Hawkesworth CJ, Moorbath S, O'Nions RK, Wilson JF (1975) Age relationships between greenstone belts and "granites" in the Rhodesian Archaean craton. Earth Planet Sci Lett 25: 251–262

Hayashi K-I, Ohmoto H (1991) Solubility of gold in NaCl- and H_2S-bearing aqueous solutions at 250–350 °C. Geochim Cosmochim Acta 55: 2111–2126

Hedenquist JW (1996) Hydrothermal systems in volcanic arcs – origin of and exploration for epithermal gold deposits. Short course notes, Mineral Resources Department, Geol Surv Jpn, 139 p

Herrington RJ (1991) The relationship between fluids and structure at the Patchway Gold Mine, Zimbabwe. PhD Thesis, Department of Geology, Royal School of Mines, Imperial College London, 378 p

Hey MH (1954) A new review of the chlorites. Mineral Mag 30: 277–292

Issigonis MJ (1980) Occurrence of disseminated gold deposits in porphyries in Archean Abitibi belt, northern Quebec, Canada. Inst Mining Met Trans 89: B: 157–158

Jelsma HA (1993) Granites and greenstones in northern Zimbabwe: tectono-thermal evolution and source regions. PhD Thesis, Vrije Universiteit te Amsterdam, Amsterdam

Jowett ETC (1991) Fitting iron and magnesium into the hydrothermal chlorite geothermometer. GAC/AGC-MAC/AMC-SEG Toronto, Prog Abstr 16: A62

Keays RR, Skinner BJ (1989) Introduction. In: Keays RR, Ramsay WRH, Groves DI (eds) The geology of gold deposits: the perspective in 1988. Econ Geol Monogr 6: 1–8

Kerrich R (1989) Geodynamic setting and hydraulic regimes: shear zone hosted mesothermal gold deposits. In: Bursnall JT (ed) Mineralization and shear zones. Geological Association of Canada, Short course notes 6, Montréal, pp 89–128

Kiba T, Takagi T, Yoshimura Y, Kishi J (1955) Tin (II) strong phasphoric acid. A new reagent for the determination of sulfate by reduction to hydrogen sulphide. Bull Chem Soc Jpn 28: 641–644

Kranidiotis P, MacLean WH (1987) Systematics of chlorite alteration at the Phelps Dodge massive sulfide deposit, Matagami, Quebec. Econ Geol 82: 1898–1911

Ludwig KR (1980) A computer program to convert raw U-Th-Pb isotope ratios to blank-corrected isotope ratios and concentrations with associated error-correlations: United States Geol Surv, Open File Rep OF-82-820

Ludwig KR (1990) ISOPLOT for MS-DOS, a plotting and regression program for radiogenic isotope data, for IBM-PC compatible computers, version 2.03: US Geol Surv, Open File Rep OF-88-0557

McCrea JM (1950) The isotopic chemistry of carbonates and a paleotemperature scale. J Chem Phys 18: 849

Marshall DJ (1987) Cathodoluminescence of geological materials. Allen and Unwin, London, 146 p

Middlemost EAK (1985) Magmas and magmatic rocks; an introduction to igneous petrology. University of Sydney, Department of Geology and Geophysics, Sydney. Longman, London, 266 p

Nutt TCH, Treloar PJ, Thorpe RI, Cummings GC (1988a) The geology and geochemistry of the gold-antimony mineralization in the Kwekwe goldfield, Zimbabwe. Bicentennial Gold '88, Melbourne: 103–106

Nutt TCH, McCourt S, Vearncombe JR (1988b) Structure of some gold and antimony-gold deposits from the Kaapvaal and Zimbabwe cratons. In: Ho SE, Groves DI (eds) Advances in understanding precambrian gold deposits, II, Geology Department and University Extension 12, The University of Western Australia, Perth, pp 63–80

Ohmoto H (1986) Stable isotope geochemistry of ore deposits. In: Valley JW, Taylor HP, O'Neil JR (eds) Stable isotopes in high temperature geological processes. Reviews in Mineralogy 16, Mineralogical Society of America, Blacksburg, Virginia, pp 491–560

Perring CS, McNaughton NJ (1992) The relationship between Archaean gold mineralization and spatially associated minor intrusions at the Kambalda and Norseman gold camps, Western Australia: lead isotope evidence. Mineralium Deposita 27: 10–22

Perring CS, Groves DI, Shellabear JN, Hallberg JA (1991) The "porphyry-gold" association in the Norseman-Wiluna Belt of Western Australia: implications for models of Archaean gold metallogeny. Precamb Res 51: 85–113

Phillips GN, Powell R (1993) Link between gold provinces. Econ Geol 88: 1084–1098

Pitfield PEJ, Campbell SDG (1990) Integrated exploration, Midlands Goldfield Project: Preliminary results. Ann Zimbabwe Geol Surv XIV: 21–33

Pitfield PEJ, Campbell SDG (1993) The structural evolution and gold mineralization of the Midlands greenstone belt, Zimbabwe (folding and granitoids). British Geol Surv – Zimbabwe Geol Surv, Technical Cooperation Project Final Rep vol 2/II: 165–301

Pitfield PEJ, Campbell SDG, Mugambate F (1991) The structural interpretation and gold-bearing potential of the Munyati shear zone, Midlands Goldfield. Ann Zimbabwe Geol Surv XV: 11–28

Porter CW, Foster RP (1991) Multi-phase ductile-brittle deformation and the role of Archaean thrust tectonics in the evolution of the Globe and Phoenix gold deposit, Zimbabwe. In: Ladeira EA (ed) Gold '91, Brazil. AA Balkema, Rotterdam, pp 665–672

Roedder E (1984) Fluid inclusions. Reviews in Mineralogy 12. Mineralogical Society of America, Blacksburg, Virginia, 646 p

Rossmann GR (1987) Spectroscopy of micas. In: Bailey SW (ed) Micas. Reviews in Mineralogy 13. Mineralogical Society of America, Blacksburg, Virginia, pp 145–182

Seward TM (1991) The hydrothermal geochemistry of gold. In: Foster RP (ed) Gold metallogeny and exploration. Blackie, Glasgow, pp 37–62

Sillitoe RH (1979) Some thoughts on gold-rich porphyry copper deposits. Mineralium Deposita 14: 161–174

Sillitoe RH (1991) Intrusion-related gold deposits. In: Foster RP (ed) Gold metallogeny and exploration. Blackie Ltd, London, pp 165–207

Sinclair WD (1980) Gold deposits of the Matachewan area, Ontario. In: Hodder RW, Petruk W (eds) Geology of Canadian gold deposits. Canadian Institute of Mining and Metallurgy, Spec vol 24, pp 83–93

Spooner ETC (1991) The magmatic model for the origin of Archean Au-quartz vein ore systems: An assessment of the evidence. In: Ladeira EA (ed) Gold '91, Brazil. AA Balkema, Rotterdam, pp 313–318

Stowe CW (1979) Gold and associated mineralisation in the Que Que area, Rhodesia. Spec Publ Geological Society South Africa 5: 39–48

Ueda A, Krouse HR (1986) Direct conversion of sulphide and sulphate minerals to SO_2 for isotope analyses. Geochem J 20: 209–212

Vila T, Sillitoe RH, Betzhold J, Viteri E (1991) The porphyry gold deposit at Marte, northern Chile. Econ Geol 86: 1271–1286

Vinyu ML, Frei R, Jelsma HA (in press) Timing between granitoid emplacement and associated gold mineralization: examples from the ca. 2.7 Ga Harare – Shamva greenstone belt, northern Zimbabwe. Can J Earth Sci

Walshe JL (1986) A sic-component chlorite solid solution model and the conditions of chlorite formation in hydrothermal and geothermal systems. Econ Geol 81: 681–703

Wilcox RE (1987) Optical properties of micas under the polarizing microscope. In: Bailey SW (ed) Micas. Reviews in Mineralogy 13. Mineralogical Society of America, Blacksburg, Virginia, pp 183–200

Zhang Y-G, Frantz JD (1987) Determination of the homogenization temperatures and densities of supercritical fluids in the system NaCl-KCl-$CaCl_2$-H_2O using synthetic fluid inclusions. Chem Geol 64: 335–350